

Qvar Sensing for Monitoring Respiration

Alyssa Chew

*Masters of Engineering, IoT Systems
University of California - Los Angeles
Los Angeles, United States of America
alyssachew@g.ucla.edu*

Varsha Senthil

*Masters of Engineering, IoT Systems
University of California - Los Angeles
Los Angeles, United States of America
vsenthil@g.ucla.edu*

Naya Menezes

*Masters of Engineering, Autonomous Systems
University of California - Los Angeles
Los Angeles, United States of America
nayamenezes21@gmail.com*

Yuchen Song

*Masters of Engineering, Autonomous Systems
University of California - Los Angeles
Los Angeles, United States of America
yuchs10@g.ucla.edu*

Abstract—Measuring respiratory rate in long-term breathing monitoring still remains difficult. The role of respiratory rate in diagnosing diseases and as an early indicator in physiological conditions is widely recognized. The purpose of this study was to determine the possibility of utilizing the ST Qvar sensor to produce a low-power device that could be utilized to accurately capture respiratory rate. A total of 4 users (1 male, 3 females) were tested in 3 positions over a 2-month period. Experiments were conducted with the Qvar-electrode system, while ground truth data was simultaneously collected utilizing a commercially available chest strap (the NeuLog Neuron Logger Sensors NUL-236 Respiration Monitor Belt Logger Sensor). Each participant took 15 samples in each of the 3 positions. The final machine learning model was able to accurately classify respiratory rates into ranges of 5 breaths per minute with 83.29% accuracy. Sitting and standing positions produced less noise than walking. Potential impacts due to subject gender and other factors have been discussed.

Index Terms—Qvar; respiratory rate; respiration; electrostatic sensors; low power consumption

I. PROBLEM DEFINITION

Qvar technology is a novel approach for biosensing applications. As developed in depth by STMicroelectronics, research has been done on using Qvar for wearables. Qvar itself functions for touch detection based on two signals, those are the QVAR1/QVAR2 and GND signals. This leads to saturation on the positive side when touching QVAR1 and GND, whereas the same occurs on the negative side when touching QVAR2 and GND. This provides the Qvar signal that can be analyzed (such as the fluctuations and variations over time) based on the application. This project aims to test the capabilities of Qvar technology for collecting respiratory data and analyzing patterns in the signal. The project setting will be the Networked & Embedded Systems Laboratory at 1762 Boelter Hall at the University of California - Los Angeles, with a consistent setup for trials to collect respiratory data from users. As this project involves evaluating the scope and effectiveness of this new approach with Qvar, it falls more under the research domain.

The problem being broken down is that there is not enough research on the capabilities of Qvar as a form of respiratory data collection and analysis. The goal of this project is to compare its performance with ground truth data from a medical device as well as differences in how it performs based on electrode placement on the body. There are several major aspects that need to be considered with this problem in mind. One of these includes how to attach the Qvar sensors to the body, such as whether to use electrodes. This also leads to the question of placement of these electrodes on the body for optimal data collection with improved information accuracy. Measurements must be taken with these different approaches to analyze the patterns for highest accuracy of analysis when compared with ground truth values captured by an existing commercial chest band. In order to evaluate performance of Qvar with different parameters, measurements will have to be taken with different settings on the app such as sampling rates, filters, and impedance. After the data collection phase, understanding how to break down the respiratory data and analyze its patterns is essential.

The Qvar technology is being used with the STMicroelectronics SensorTile.box PRO device and can be paired with the corresponding Android app for development and data collection. The environment will be controlled, and all trials will take place in the Networked & Embedded Systems Laboratory with the same setup with different participants for comprehensive data collection. The main possible limitations to consider include time as well as variations in data collected from different people. With research, the aim is to build on existing frameworks of current respiratory data collection and analysis methods to explore the capabilities of Qvar technology.

The starting hypothesis is that Qvar will perform slightly lower than the commercial sensor (NeuLog Neuron Logger Sensors NUL-236 Respiration Monitor Belt Logger Sensor) in terms of accuracy; however, it will allow for a more flexible and lower-power consumption design for users. In addition, signal processing and machine learning can help



Fig. I.1. SensorTile.box PRO with Qvar Technology [11]

with more detailed analysis of the respiratory patterns. The main variables to consider include the sensors used: NeuLog Neuron Logger Sensors NUL-236 Respiration Monitor Belt Logger Sensor, Qvar with radar, Qvar with electrodes as well as placement of electrodes: two electrodes on the chest, two on the ribs, one on the right chest and one on the left rib, one on the left chest and one on the right rib, or a singular electrode. Analysis into balancing hardware, signal processing, and machine learning can also be assessed. Understanding the strengths and limitations of each aspect and how they can be combined to obtain interpretable data is essential for this study. With this research, the capabilities of Qvar technology can be explored further in the field of biosensing. Respiratory data collection and analysis methods can also be compared to find the method that provides respiratory rate characteristics closest to ground truth values (taken with NeuLog Neuron Logger Sensors NUL-236 Respiration Monitor Belt Logger Sensor). With these strategies, further understanding and processing of Qvar signals in bio-applications can be achieved.

II. PROBLEM SCOPING (LITERATURE REVIEW)

In the study conducted in this paper, the STMicroelectronics SensorTile.box PRO is tested to determine whether it is capable of measuring respiratory frequency to produce results accurately compared to ground truth (collected using NeuLog Neuron Logger Sensors NUL-236 Respiration Monitor Belt Logger Sensor). This is done by collecting data using both the Qvar sensors and NeuLog Neuron Logger Sensors NUL-236 Respiration Monitor Belt Logger Sensor simultaneously for comparison. If shown to be possible, the SensorTile.box PRO could then be used in the wide range of applications that require respiratory frequency monitoring. There is an increasing need to measure respiratory variables for many

applications, and there are many different ways to go about it, using several different sensors.

A. Contact-Based Methods for Measuring Respiratory Frequency

In a paper by Carlo Massaroni published in Sensors Journal of Multidisciplinary Publishing Institute (MDPI), an overview of the available contact-based methods for measuring respiratory frequency is presented as well as a summary of the importance of monitoring respiratory frequency. Respiratory frequency is an early indicator of physiological deterioration and can be a predictor for other adverse events like cardiac arrest. It is also useful in detecting conditions like sleep apnea or respiratory depression, and is sensitive to many other conditions [8]. With the arrival of COVID-19, a possible application of monitoring respiratory frequency is the ability to detect COVID-19 early as well. Monitoring respiratory biomarkers is also useful in occupational settings as it is sensitive to stress, pain, environmental challenges, and other factors that can allow companies to look into improving safety and health. Of course, in addition to this, tracking respiratory frequency during exercise and sports training is also an important application that assists in determining exertion levels [8]. In addition to these applications discussed above from Massaroni's summary, there are many other applications where measuring respiratory rate is necessary or useful.

In terms of the many different sensors currently available that are capable of measuring respiratory frequency, the choice of which one to use does depend on the application. Factors to consider include sensitivity, step response time, output linearity, accuracy, size, cost, real-time monitoring, measurement intrusiveness, sensitivity to body motion not related to breathing, environmental factor influence, and wire presence [8]. In the overview done by Massaroni, contact-based methods are the focus. One contact-based technique is based on respiratory airflow. This involves using different sensors to measure the velocity or volume of air as it is inhaled and exhaled, which then allows for an estimate of the respiratory frequency [8]. Sensors used for this include differential flowmeters, turbine flowmeters, hot wire anemometers, and fiber-optic-based flowmeters. The metrological properties and sensor characteristics of each sensor rated good, sufficient, and poor as done by Massaroni in the paper are shown in Table 2.1. Differential flowmeters are more solid in comparison to hot wire anemometers, which are much more fragile. Turbine flowmeters are unaffected by humidity, temperature or altitude. Fiber-optic-based flow meters have many advantages, but are in an early stage in their use in this field. The main advantage of respiratory airflow methods is accuracy, while the main disadvantage is intrusiveness. This technique is well suited to hospital settings, indoor/structured occupational settings, or indoor/structured sports settings, but can be used in a sufficient manner for daily activity monitoring for clinical settings, outdoor/unstructured occupational settings, or outdoor/unstructured sports settings [8].

TABLE I
RESPIRATORY AIRFLOW METHOD SENSOR METROLOGICAL PROPERTIES AND SENSOR CHARACTERISTIC RATINGS

| | | Differential Flowmeters | Turbine Flowmeters | Hot Wire Anemometers | Fiber-Optic Sensors |
|-------------------------|--|----------------------------|--------------------|----------------------|---------------------|
| Metrological Properties | Sensitivity | Good | Good | Good | Good |
| | Step Response Time | Good | Good | Good | Good |
| | Output Linearity | Good (depending on sensor) | Good | Poor | Good |
| | Accuracy | Good | Good | Good | Good |
| Sensor Characteristics | Sensor Size | Sufficient | Good/Sufficient | Sufficient | Good |
| | Cost | Sufficient | Sufficient | Sufficient | Poor |
| | Real-Time Monitoring | Good | Good | Good | Good |
| | Measurement Intrusiveness | Sufficient | Sufficient | Sufficient | Sufficient |
| | Sensitivity to Motion Outside of Breathing | Good | Sufficient | Poor | Poor |
| | Environmental Influence | Good | Good | Good | Sufficient |
| | Presence of Wire | Poor | Sufficient | Sufficient | Poor |

Another contact-based method is based on respiratory sounds. This method uses the sound created by air flowing through the throat to estimate respiratory frequency by looking at the inspiration and expiration phases of breathing [8]. Respiratory sounds are usually observed using acoustic sensors (microphones) that convert the acoustic pressure variations to electrical signals. The metrological properties and sensor characteristics of microphones rated as good, sufficient, and poor as done by Massaroni in the paper are shown in II. This method is useful because it can be placed in wearable devices, with unobtrusiveness being its main advantage. However, microphones tend to pick up background noise, making environmental influence its main disadvantage. This method is not recommended for measurement of the respiratory waveform overtime [8]. This technique performs sufficiently in hospital settings, home activity monitoring uses, indoor/structured occupational settings, or indoor/structured sports settings, but poorly in outdoor/unstructured occupational settings or outdoor/unstructured sports settings [8].

TABLE II
RESPIRATORY SOUNDS METHOD SENSOR METROLOGICAL PROPERTIES AND SENSOR CHARACTERISTIC RATINGS

| | | Microphones |
|-------------------------|--|---|
| Metrological Properties | Sensitivity | Good |
| | Step Response Time | Good |
| | Output Linearity | (depending on sensor) |
| | Accuracy | Good |
| Sensor Characteristics | Sensor Size | Good |
| | Cost | Good |
| | Real-Time Monitoring | Sufficient |
| | Measurement Intrusiveness | Good |
| | Sensitivity to Motion Outside of Breathing | Good |
| | Environmental Influence | Poor |
| | Presence of Wire | (depending on location of sensor on body) |

The next contact-based method discussed in Massaroni's paper is based on air temperature, where the difference in

temperature between air inhaled and exhaled can be used to estimate the respiratory frequency. Types of sensors used in this method include thermistors, thermocouples, pyroelectric sensors, and fiber optic sensors. Thermistors have a slower response time compared to the others. Fiber-optic sensors require wires for power supply and light delivery [8]. The metrological properties and sensor characteristics of the sensors rated as good, sufficient, and poor as done by Massaroni in the paper are shown in III. Temperature sensors are placed near the nostrils or lips and are often integrated into face masks. Overall, these sensors are sensitive to environmental factors and have a high presence of wires, making their applicability limited to controlled environments [8]. This method's main advantage is the sensitivity, while its main disadvantage is its intrusiveness. This method is well-suited to hospital settings. This technique performs sufficiently in home activity monitoring uses, indoor/structured occupational settings, or indoor/structured sports settings, but poorly in outdoor/unstructured occupational settings or outdoor/unstructured sports settings [8].

Another contact-based technique for measuring respiratory frequency is based on air humidity, where the respiratory signal is estimated based on the difference in the water vapor contents between the inhaled and exhaled air [8]. The types of sensors used here include capacitive sensors, resistive sensors, nanocrystals or nanoparticle sensors, and fiber-optic sensors. Capacitive sensors are most commonly used in this application, while fiber-optic sensors and nanoparticle technology are up and coming in attracting research attention [8]. The metrological properties and sensor characteristics of the sensors rated as good, sufficient, and poor as done by Massaroni in the paper are shown in IV. These sensors are rather invasive but small in size. They are usually around the nostril or the mouth. They can be used to measure the respiratory waveform over time. These sensors have only been used in structured environments rather than other applications [8]. This method has the main advantage of having low sensitivity to movement outside of breathing, while its main disadvantage is the intrusiveness of the location of the sensor. This technique performs sufficiently in hospital settings, home activity monitoring uses,

TABLE III
AIR TEMPERATURE METHOD SENSOR METROLOGICAL PROPERTIES AND SENSOR CHARACTERISTIC RATINGS

| | | Thermistors | Thermocouples | Pyroelectric Sensors | Fiber-Optic Sensors |
|-------------------------|--|-------------|---------------|----------------------|---------------------|
| Metrological Properties | Sensitivity | Good | Good | Good | Good |
| | Step Response Time | Sufficient | Good | Good | Good |
| | Output Linearity | Good | Good | Good | Good |
| | Accuracy | Good | Good | Good | Good |
| Sensor Characteristics | Sensor Size | Sufficient | Good | Good | Good |
| | Cost | Good | Sufficient | Sufficient | Poor |
| | Real-Time Monitoring | Sufficient | Good | Good | Good |
| | Measurement Intrusiveness | Sufficient | Sufficient | Sufficient | Sufficient |
| | Sensitivity to Motion Outside of Breathing | Good | Good | Good | Good |
| | Environmental Influence | Poor | Poor | Poor | Poor |
| | Presence of Wire | Poor | Poor | Poor | Poor |

indoor/structured occupational settings, or indoor/structured sports settings, but poorly in outdoor/unstructured occupational settings or outdoor/unstructured sports settings [?].

Respiratory frequency can also be estimated by comparing the amount of oxygen and carbon dioxide in the inhaled and exhaled air that occurs because of cellular respiration. The sensors that are used for this method include infrared sensors and fiber-optic sensors. Infrared sensors are most commonly used in clinical settings and during indoor sports. The metrological properties and sensor characteristics of the sensors are rated as good, sufficient, and poor as done by Massaroni in the paper are shown in V. Overall, this method places sensors near the nose and lips, typically using face masks [8]. One of the issues of this method is its sensitivity to environmental factors and other gas components. These sensors can be used for continuous monitoring of the respiratory waveform overtime. The main advantage of this method is the accuracy, while the main disadvantage is its intrusiveness. [8]. This method is well-suited to hospital settings and indoor/structured occupational settings. This technique performs sufficiently in home activity monitoring uses and indoor/structured sports settings, but poorly in outdoor/unstructured occupational settings and outdoor/unstructured sports settings [8].

Another common contact-based method to measure the respiratory frequency and waveform is based on the movement of the chest as the diaphragm expands and contracts. This can be done using strain sensors, impedance sensors, or movement sensors. Strain sensors are used to convert the cyclic expansion and contraction of the chest to extract a breathing pattern and respiratory frequency [8]. Types of strain sensors include resistive sensors, capacitive sensors, inductive sensors, and fiber-optic sensors. The metrological properties and sensor characteristics of the sensors are rated as good, sufficient, and poor as done by Massaroni in the paper are shown in VI. In terms of impedance sensors, transthoracic impedance sensors are used. The properties and characteristics of impedance sensors are rated in VII. There are three main kinds of movement sensors used to record data related to chest movement: accelerometers, gyroscopes, and magnetometers. Accelerometers measure

acceleration forces caused by motion. Gyroscopes measure the angular velocity if the frame is rotating. Magnetometers are magnetic field sensors. The metrological properties and sensor characteristics of the movement sensors are rated as good, sufficient, and poor as done by Massaroni in the paper are shown in VIII. These movement sensors are present in the IMU sensor in the SensorTile.box PRO which are being tested during the study of this capstone project. Overall, strain and movement sensors can be placed in wearable devices and clothes and are not invasive, which is the main advantage of this method [8]. Sensors need to be placed near the upper chest. The main disadvantage is that these sensors are sensitive to movement other than breathing. Strain measurements are well-suited for hospital settings, at home/daily activity monitoring, indoor and outdoor occupational settings, and indoor and outdoor sport settings. Impedance measurements are well suited for hospital settings and indoor/structured occupational settings. They perform to a sufficient level in daily activity monitoring and indoor/structured sport settings but poorly in outdoor/unstructured occupational settings and outdoor/unstructured sport settings. This method using movement measurements is sufficient for hospital settings, at home/daily activity monitoring, indoor and outdoor occupational settings, and indoor/structured sport settings but is poor for outdoor/unstructured sport settings [8].

Another type of contact-based method for measuring respiratory frequency is based on the modulation of cardiac activity. This is done using electrocardiography (ECG) or photoplethysmography (PPG). ECG measures electrical activity due to action potentials in heart muscle. PPG measures changes in blood volume over time. The metrological properties and sensor characteristics of the sensors are rated as good, sufficient, and poor as done by Massaroni in the paper are shown in IX. The main advantage of these is they are unobtrusive, but the disadvantage is they are susceptible to picking up motion outside of breathing [8]. This method is well-suited to hospital settings. It is sufficient for daily activity monitoring and indoor/structured occupational and sport settings. It is poor for outdoor/unstructured occupational and sport settings [8].

TABLE IV
AIR HUMIDITY METHOD SENSOR METROLOGICAL PROPERTIES AND SENSOR CHARACTERISTIC RATINGS

| | | Capacitive Sensors | Resistive Sensors | Nanocrystals/ Nanoparticles | Fiber-Optic Sensors |
|-------------------------|--|--------------------|-------------------|--------------------------------|---------------------|
| Metrological Properties | Sensitivity | Good | Good | Good | Good |
| | Step Response Time | Poor | Sufficient/Poor | Good/Sufficient | Good/Sufficient |
| | Output Linearity | Good | Good | Good | Good |
| | Accuracy | Good | Good | Good | Good |
| Sensor Characteristics | Sensor Size | Sufficient | Sufficient | Sufficient | Good |
| | Cost | Good | Good | Sufficient | Poor |
| | Real-Time Monitoring | Good | Good | Good | Good |
| | Measurement Intrusiveness | Sufficient | Sufficient | Sufficient | Sufficient |
| | Sensitivity to Motion Outside of Breathing | Good | Good | Good | Sufficient |
| | Environmental Influence | Poor | Poor | Poor | Sufficient |
| | Presence of Wire | Poor | Poor | Poor | Poor |

TABLE V
AIR COMPONENTS METHOD SENSOR METROLOGICAL PROPERTIES AND SENSOR CHARACTERISTIC RATINGS

| | | Infrared Sensors | Fiber-Optic Sensors |
|-------------------------|--|------------------|---------------------|
| Metrological Properties | Sensitivity | Good | Good |
| | Step Response Time | Good | Good |
| | Output Linearity | Good | Good |
| | Accuracy | Good | Good |
| Sensor Characteristics | Sensor Size | Sufficient | Good |
| | Cost | Sufficient | Sufficient/Poor |
| | Real-Time Monitoring | Good | Good |
| | Measurement Intrusiveness | Sufficient | Sufficient |
| | Sensitivity to Motion Outside of Breathing | Good | Good |
| | Environmental Influence | Poor | Poor |
| | Presence of Wire | Poor | Poor |

As shown in the discussion above, there are many different methods and sensors that can be used to measure respiratory waveforms. This capstone project looks into whether or not the SensorTile.box PRO's Qvar capabilities allow it to be added to these applications and possibilities.

B. Telemonitoring Systems for Respiratory Patients

In another study conducted by Alessandra Angelucci, telemonitoring systems for respiratory patients are presented. Telemonitoring systems currently use a “two-hop architecture” where data from the sensors are transmitted to sensor-manager technologies and then to data management [1]. Spirometers are one of several types of sensors often used for respiratory monitoring. In the telemonitoring world, handheld spirometry devices are most suitable and are often connected to a smartphone. The issue with this is that only infrequent assessments are possible due to the requirement of a mask or tube. Another technique is forced oscillation, which is noninvasive and measures lung function by using small pressure oscillation [1]. Wearable systems that can continually measure breathing include respiratory inductance plethysmography (RIP), resistance-based wearable sensors, capacitance-based wearable sensors, inertial measurement units, and fiber optic sensors.

RIP uses transducer bands to monitor the chest and abdomen. As the subject breathes, the volume of the compartments changes and the alterations in the self-inductance of the coils reflect those changes [1]. Resistance-based wearable sensors rely on the movement of the torso and often use accelerometer and strain sensors [1]. Capacitance-based wearable sensors use variations in electrical capacity to obtain respiratory patterns [1]. Inertial measurement units similarly to resistance-based sensors use movement. They use the movement of the rib cage to produce the respiratory waveform. Fiber-optic sensors have shown promising results to monitor respiratory rates by integrating them into sensing elements in patches or garments [1]. There are also non-wearable devices that can be embedded within individuals to monitor respiration like ventilators and such. There have also been promising results in contactless methods in telemonitoring techniques like Doppler bio-radars to monitor physiological signals [1].

In addition to respiration, other biomarkers must be measured in respiratory patients. This includes oxygen concentrations. Pulse oximeters are used for that. Low blood oxygen increases the risk of “respiratory exacerbation” [1]. Pulse oximeters use spectrophotometric methodology by illuminating portions of the skin and measuring light absorption, which depends on the level of oxygenated blood [1]. Commonly, finger pulse oximeters are used, but this can be done on different parts of the body (e.g. wrist, head, leg, etc.). There are also non-contact methods using phone or computer cameras, where the skin must be in front of a camera lens for several seconds to get the same results [1].

In the world of telemonitoring, one of the other devices that is commonly used is activity monitors. They often have algorithms for automatic recognition and can be used to evaluate a whole process rather than specific moments in time. There are currently sensor-based, vision-based, and radio-based systems [1]. Sensor-based systems use micro-electro-mechanical systems. They can contain any combination of accelerometer, gyroscopes, magnetometers, and barometric pressure sensors to monitor the body’s movement. Video-based recognition systems often use RGB video, depth video, and

TABLE VI
STRAIN SENSOR METROLOGICAL PROPERTIES AND SENSOR CHARACTERISTIC RATINGS

| | | Resistive Sensors | Capacitive Sensors | Inductive Sensors | Fiber-Optic Sensors |
|-------------------------|--|-------------------|--------------------|-------------------|---------------------|
| Metrological Properties | Sensitivity | Good | Good | Good | Good |
| | Step Response Time | Good | Good | Good | Good |
| | Output Linearity | Sufficient | Sufficient | Sufficient | Sufficient |
| | Accuracy | Good | Good | Good | Good |
| Sensor Characteristics | Sensor Size | Good | Good | Sufficient | Good |
| | Cost | Good | Good | Good | Sufficient |
| | Real-Time Monitoring | Good | Good | Good | Good |
| | Measurement Intrusiveness | Good/Sufficient | Good/Sufficient | Good/Sufficient | Good/Sufficient |
| | Sensitivity to Motion Outside of Breathing | Poor | Poor | Sufficient | Poor |
| | Environmental Influence | Sufficient | Good | Good | Good |
| | Presence of Wire | Good | Good | Sufficient | Sufficient |

TABLE VII
IMPEDANCE SENSOR METROLOGICAL PROPERTIES AND SENSOR CHARACTERISTIC RATINGS

| | | Transthoracic Impedance Sensor |
|-------------------------|--|--------------------------------|
| Metrological Properties | Sensitivity | Good |
| | Step Response Time | Good |
| | Output Linearity | Good |
| | Accuracy | Good |
| Sensor Characteristics | Sensor Size | Good |
| | Cost | Good |
| | Real-Time Monitoring | Good |
| | Measurement Intrusiveness | Sufficient |
| | Sensitivity to Motion Outside of Breathing | Poor |
| | Environmental Influence | Good |
| | Presence of Wire | Sufficient |

RGB-D video to recognize complex gait activities. However, these systems are often limited in range due to camera range limitations [1]. Radio-based recognition systems use radio frequencies to detect positioning, most often RFID and Wi-Fi [1].

In addition to activity monitoring, there are wearable devices that can measure air quality both indoors and outdoors which are important variables in respiratory research. In the case of respiratory patients, the parameters of interest include concentration of CO₂, CO, NO₂, O₃, fine particles, and chemical and microbiological volatile organic compounds [1]. They also study the impacts of temperature and humidity. Other physiological parameters that are monitored include PaCO₂ and tcpCO₂, heart rate using electrocardiographs, arterial blood pressure, and temperature [1].

Telemonitoring communication system sensor-manager link technologies include Bluetooth and Bluetooth low energy (BLE), ANT and ANT+ which use ultra-low-power and short-range wireless communications, Z-Wave which is a wireless communication standard for remotely controlled applications, and ZigBee which is widely used in WBANs [1]. In terms of cellular link technologies, the commonly used ones are Wi-Fi,

4G, and 5G.

These telemonitoring communication systems were tested in many clinical studies on chronic respiratory patients, predominantly with people with COPD, asthma, and cystic fibrosis [1]. The main issue with the studies covered in the paper is that they do not collect all the parameters of interest and rather only a few of them, and often do not use telemonitoring fully and analyze data offline rather than in real time. Overall, the field of telemonitoring can bring benefits in terms of quality and economic aspects [1].

As shown in the discussion above, there are many different methods and sensors used in telemonitoring, particularly for use with respiratory patients. This capstone project looks into whether or not the SensorTile.box PRO's Qvar capabilities allow it to be added to these applications and possibilities.

C. Strain Sensors Use in Measuring Respiration Rate and Volume

In another study done by Michael Chu published in Nature Journal Digital Medicine, strain sensors were utilized to observe respiration rate and volume measurements [3]. The focus of their study was to demonstrate that it was possible to measure respiration rate and volume by using a wearable strain sensor placed on the rib cage and abdomen. This is similar to the project being done for the capstone, where the focus is whether the Qvar sensor is capable of taking respiration rate measurements. The size of the sensor used in Chu's study was smaller than a typical Band-Aid [3]. For each subject, a calibration model was developed allowing for the calculation of the respiration volume. A proof of concept was also created to show that the strain sensors were capable of recording respiration signals when subjects were walking or running. Subjects were also tested using a tethered data acquisition unit for data alignment purposes. It was also demonstrated that wireless respiration monitoring was possible through Bluetooth [3].

The strain sensors used in this study were made of a "piezo-resistive metal thin film set in a silicone elastomer substrate" [3]. The sensor works in regard to the "controlled fracturing of the metal film to increase resistance with respect to strain"

TABLE VIII
MOVEMENT SENSOR METROLOGICAL PROPERTIES AND SENSOR CHARACTERISTIC RATINGS

| | | Accelerometers | Gyroscopes | Magnetometers |
|-------------------------|--|----------------|------------|---------------|
| Metrological Properties | Sensitivity | Good | Good | Good |
| | Step Response Time | Good | Good | Good |
| | Output Linearity | Good | Good | Good |
| | Accuracy | Good | Good | Good |
| Sensor Characteristics | Sensor Size | Good | Good | Good |
| | Cost | Good | Good | Good |
| | Real-Time Monitoring | Good | Good | Good |
| | Measurement Intrusiveness | Good | Good | Good |
| | Sensitivity to Motion Outside of Breathing | Poor | Poor | Poor |
| | Environmental Influence | Good | Good | Sufficient |
| | Presence of Wire | Good | Good | Good |

TABLE IX
BIOPOTENTIAL SENSOR METROLOGICAL PROPERTIES AND SENSOR CHARACTERISTIC RATINGS

| | | ECG | PPG |
|-------------------------|--|------------|------|
| Metrological Properties | Sensitivity | Good | Good |
| | Step Response Time | Good | Good |
| | Output Linearity | Good | Good |
| | Accuracy | Sufficient | Good |
| Sensor Characteristics | Sensor Size | Good | Good |
| | Cost | Sufficient | Good |
| | Real-Time Monitoring | Good | Good |
| | Measurement Intrusiveness | Sufficient | Good |
| | Sensitivity to Motion Outside of Breathing | Sufficient | Poor |
| | Environmental Influence | Sufficient | Good |
| | Presence of Wire | Sufficient | Good |

[3]. The maximum strain the sensors chosen could withstand was well above what was needed for measuring respiration. These sensors were placed on the rib cage and abdomen. They measured the contraction and expansion of these locations as the subject was breathing. These sensors were 21mm by 10mm by .5mm by .5mm by .5mm by .5mm [3]. Eight participants were chosen. Five of them were men, and three of them were women. Height, weight, and blood pressure were recorded prior to sensor placement. The accelerometer was set below the sternum and the spirometer was held using a head strap. There were several different tests and procedures done. The calibration procedure consisted of one minute of shallow breathing, one minute of medium breathing, and one minute of deep breathing. For paced respiration, an audio-visual metronome was used to which participants had to match their breathing. For test respiration, participants could take any sequence of shallow, medium, and deep breaths of their choosing. For the pulmonary function test, participants inhaled to maximum capacity and exhaled forcefully for a set duration. The last participant was tested under walking and running conditions as well [3].

The results of the study showed that the strain sensors were able to calculate the respiration rate and volume based on the

changes in strain at the local areas of the abdomen and rib cage where the sensors were placed [3]. This was for sedentary conditions. This matches other research suggesting that the movement in those areas would be proportional to the volume of air inhaled and exhaled [3]. The movement on either side of the rib cage and abdomen should also be symmetric [3]. The data taken when the subject was moving also showed that the strain sensor was able to detect a respiration signal; however, the calculated respiration volume did not match well with the measured volume. This is most likely due to the fact that strain sensors are sensitive to other motions not associated with breathing. Michael Chu's study demonstrated that strain sensors can be used to measure respiration rate and volume, and now in this project, the goal is to show that Qvar can also be used in a similar capacity. The limitations of Chu's study include the small, healthy population. This is also a limit of the testing in this study as explained in Chapter Three with four participants all of similar age and all in good health. Another limitation of Chu's study was the majority of testing was done while subjects were sedentary.

D. Cardiac Monitoring with Qvar sensor device

Another study looked into cardiac monitoring with Qvar. Digital interventions to monitor patient status are being researched to help physicians detect early indicators of deteriorating health so they can intervene. The 2022 study conducted by Dheman et al. looked to use Qvar with a wearable sensor device that can be worn underneath clothing to monitor cardiac activity. They evaluated signal quality and power consumption in comparison to other sensors currently available.

Since most consumer cardiac monitors do not provide continuous monitoring, this study looked to specifically capture long-term data, so that physicians would be able to see intermittent or transient events. Because their device would provide continuous monitoring, power consumption was a concern. Since Qvar requires little power, it is perfect for a wearable device.

The Dheman et al. study transferred data over BLE to an application that could view data in real time on an android phone. The hope is to follow a similar approach in this

experiment's data. Dheman et al. optimized the electrode positions by testing four different positions.

They also experimented with five different use case scenarios: sitting, standing, walking, running and exercise (push-ups). In the study discussed in this paper, the plan is to continue this experimentation and test electrode position as well as three different use cases (sitting, standing, and walking).

The cardiac chest strap was compared to the PPG and ECG reference sensors X [4]. The goal was to use the least power possible, so the Qvar sensor was evaluated on how well it detected the Q, R and T peaks [4]. This strap was only evaluated on two subjects, and the slight variations are likely attributable to their difference in BMI and age [4].

Dheman et al. tested their system for chest, finger and wrist wearable applications. While it was able to recreate QRS and T waveforms in the chest position, it was not able to match the accuracy as a finger or wrist wearable [4]. The Qvar based chest strap was also shown to be very sensitive to motion and saw major degradation during running [4].

TABLE X
POWER CONSUMPTION OF THE DIFFERENT SENSORS [4]

| Sensor | Voltage | Current | Power |
|--------|---------|--------------|--------------|
| QVAR | 2.53V | 34.5 μ A | 87.3 μ W |
| ECG | 3.29V | 116 μ A | 382 μ W |
| PPG | 3.29V | 7.69mA | 25.3mW |

Qvar consumes much less power than the ECG or the PPG, so if it can measure respiratory signals accurately, it would be a good solution for longer-term measurements.

E. Long-Term Polygraphic Monitoring with Qvar Sensor Device

To better understand the Qvar sensors and possible applications, another study that was looked into was conducted by Manoni et al. that aimed to determine whether a wireless wearable system could be created to provide long-term monitoring of an ECG and single-channel scalp electroencephalogram (EEG) from the frontal lobes. Since EEGs and ECGs tend to require trained personnel in hospitals or clinics, recent research has focused on creating wearable alternatives that require lower power and can be used longer term at home.

The method proposed by Manoni et al. is able to record data directly on an SD card or wirelessly. Their setup involved electrodes, wires, and a battery-powered sensor to simply test the "ST-Qvar feasibility in biopotentials acquisition" [7]. This study listed cost-effectiveness and high sensitivity as two clear advantages of using ST-Qvar as opposed to other methodologies [7].

Since Manoni et al. was evaluating EEGs and ECGs taken from ST-Qvar, a similar hardware setup was chosen for this experiment. Manoni et al. also chose to utilize a high-pass filter to eliminate DC and electrodes offset. Since they experimentally verified the appropriate cutoff frequencies, this study aims to continue this work and experiment with different filters to best capture respiratory rate and data.

Qvar data in Manoni et al.'s study was taken as the difference between two inputs. The plan is to utilize this same methodology to determine the common mode gain, from which the respiratory rate can be derived.

Similarly to Manoni et al., there is concern about potential noise in the system. Since Qvar is a low power device, and the plan is to experiment with electrodes placed directly on the skin, there is concern about the high impedance of the skin. Manoni et al. noted that dry electrodes tend to produce even more noise than wet electrodes. Since the plan is to use dry electrodes, the concern is that most of the data will also be noisy. As such, the plan is to test different methods and try different software packages to try to overcome the noise.

Similarly to Manoni et al., the plan is to try multiple setups and boards. While Manoni et al. utilized these setups to gauge whether longer term transmissions were possible, the plan is to limit the study to collecting data in 1 minute samples rather than longer transmissions. Additionally, the plan is to collect data solely to the SD card rather than via Bluetooth without the use of additional BLE hardware.

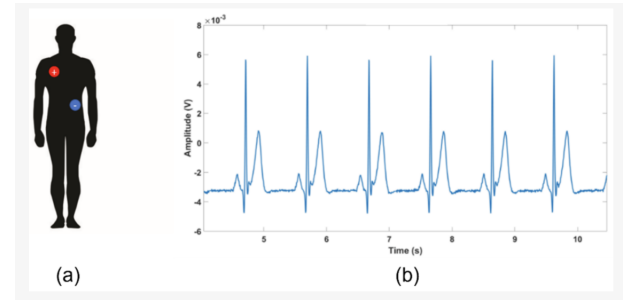


Fig. II.1. (a) Electrode placement, (b) Sample electrode waveform [7]

Manoni et al. focused their research across three different measurements, a single lead ECG, a single-channel EEG and rapid eye movement detection. For the purposes of the current experiment, it was decided to focus on respiratory rates based on an ECG system. Because of this, a similar ECG setup (RA-LL) to Manoni et al was picked, as shown in II.1.

Since the study conducted by Manoni et al. focused on static subjects, it was decided to build upon their research and additionally evaluate subjects in a walking motion. From this work, the proposed plan should be able to yield fairly accurate breathing rates and should be able to eliminate noise from the signals. As shown in II.2, Manoni et al. was able to reproduce similar results as the MicroMed device. The plan for the study is to compare the obtained results to data from a commercially available chest band.

F. Knitted Piezoresistive Smart Chest Band

Finally, a paper on knitted piezoresistive smart chest bands was looked into. Respiration patterns are useful for detecting disease early on and for analyzing psychosomatic conditions. Since people are more commonly hoping to measure these patterns outside of the hospital, they are more commonly being embedded in wearable materials. Raji et al. chose to study a

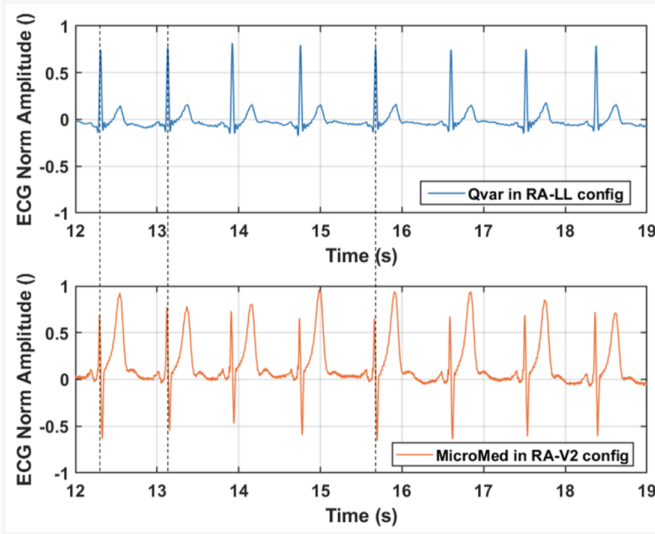


Fig. II.2. (above) Qvar in RA-LL configuration, (below) MicroMed in RA-V2 configuration [7]

knitted piezoresistive smart chest band across 20 users in a 67 day period across several test conditions. This band showed some success, with less noise during sedentary positions [9]. The results suggest that breath patterns can be used as a biometric feature. It is intended to continue this work using the Qvar sensor.

Most breathing sensors have been placed in a band around the chest since it is most accurate, but other positions are being experimented with (e.g. wrist, bed, and chair backrest). Respiratory patterns are known to vary based on age, gender, ethnicity, physical condition, stress, psychosomatic disorders, and emotions / affect. Many of the current devices are less accurate on moving subjects, so this study looked to expand the dataset across various individuals under varied conditions and activities [9].

During assessment tests, this system consisted of the belt itself, the signal acquisition, processing and transmission system (in a box attached to the belt), and a computer, connected to the system via Bluetooth, as shown in II.3.

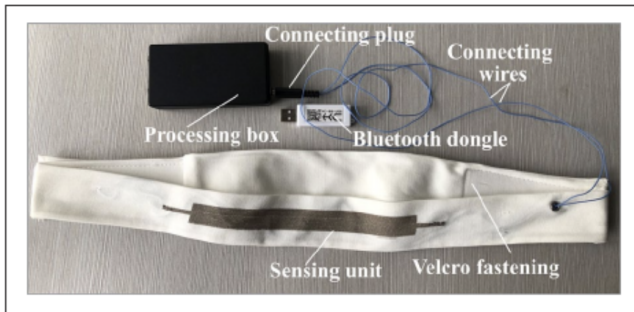


Fig. II.3. Prototype of chest band system [9]

Breathing cycles are defined as the time from the start of the inhalation to the end of the exhalation [9]. Counting the

number of times the chest rose in a minute of testing (and matching this count to the number of peaks recorded) allowed Raji et al. to determine the respiratory cycle. The volume of gas inhaled / exhaled was referred to as the breath volume. This describes the volume of gas inhaled or exhaled from a person's lungs per minute. It has a specific relationship with blood carbon dioxide levels, which has significance in respiratory medicine. The inspiratory duty cycle was used to estimate the consistency of the respiratory cycle. However, it was determined that this measure could not be used alone since it was affected a lot by a variety of factors including physical activity and partial airway obstruction [9].

The smart band was wrapped around the base of the chest for users with the same length of conductive fabric tightened across each subject. The subjects were tested 3 times in a day (morning, afternoon and evening) and across different conditions (standing, sitting and reading). Standing and sitting positions saw identical results as commercial respiration systems. However, some of the patterns saw higher levels of noise, but the sensor still performed well once the signal had been processed [9]. With the system setup in the study, the hope is to test subjects across different conditions (standing, sitting and walking).

Posture was found to have an effect on breathing cycles, where standing produced higher values (increased lung volumes), which was attributed to the increase of volume of the chest cavity. Reading activity was found to be unique from sitting and standing. These patterns show that future work could move into the area of speech production [9]. The hope is to recreate these differences in the experiments and compare the breathing values between walking and sitting/standing.

The difference in gender was similar to that of previous works, as shown in II.4 II.5. Men tend to have 10%-12% higher lung volume provided that the man and woman in question are of the same height and age [9]. However, the differences were not significant. In the proposed study, it is unlikely that there will be distinguishable gender differences from other physiological differences due to smaller sample size.

Since the study looked at people of both African and Asian descent, the impact of ethnicity was also studied. Overall, it was concluded that physique has a much larger impact on the breathing cycle.

Individual breathing rates and volumes seemed distinctively different and were influenced by physical attributes (weight, height). This indicates that the respiratory patterns and duty cycles can potentially be utilized for biometric identification in the future [9].

Age was not closely studied in this experiment because most of the subjects were between 23 and 29 years of age. Similarly, in the proposed study, the four subjects will be between ages 21 and 23 years of age.

The impact of physical activity was analyzed, as shown in II.6. The signals were much noisier (as concluded by previous studies), so Raji et al. chose to instead collect this data immediately after exercise. Rather than study moderate to

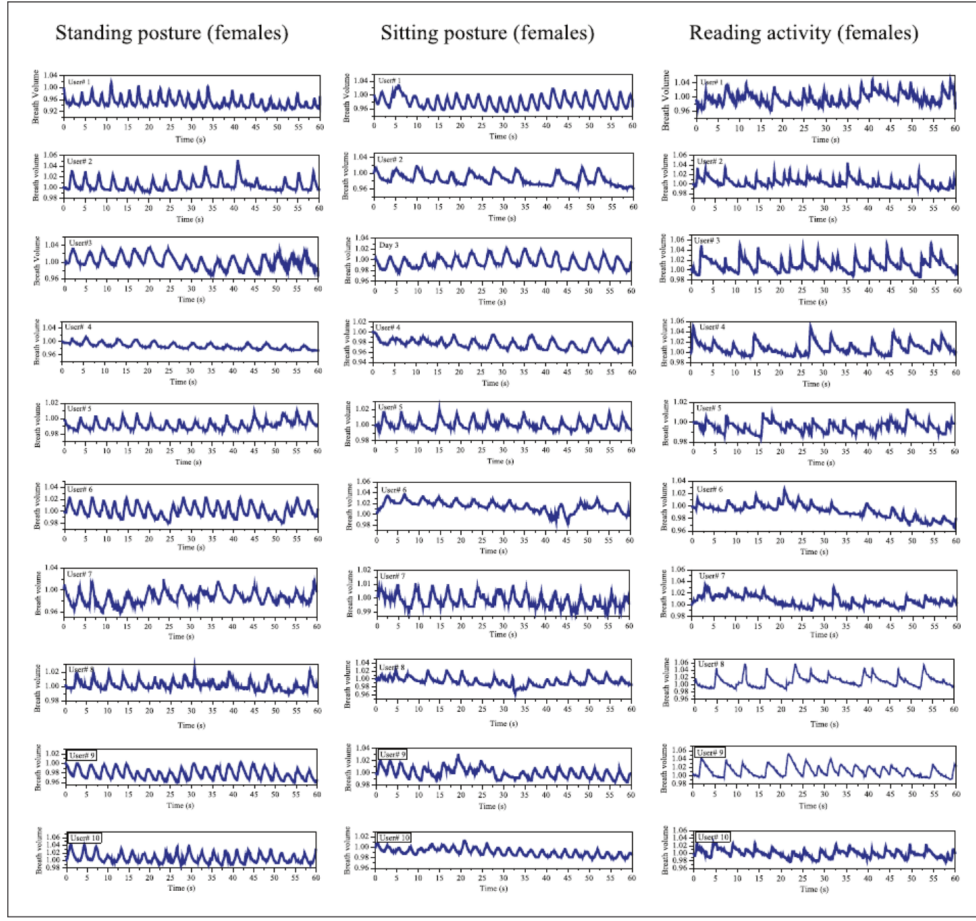


Fig. II.4. Respiration patterns of female users adduced during standing, sitting postures, and reading activities [9]

intense physical activity, this study will look into the difference between casual walking and stationary (sitting and standing) positions.

There was no clear pattern found from analyzing data taken at 3 different times of day. The results appeared to be very individual, so time of day likely has little impact on the respiratory cycle.

Finally, although height and weight have an impact on the respiratory cycle, it appears that the effect of Body Mass Index (BMI) is only obvious once the BMI exceeds 30 [9].

There were several aspects that produced noise, presenting limitations on the study. Clothing that the user wore sometimes changed the device's ability to remain stable, resulting in noisier signals. Additionally, movement and the sensor itself produced some level of noise [9]. The plan is to utilize these findings in taking data and experiment with differences in clothing as well.

The above studies provide a foundation for recreating a similar system using the Qvar sensor to accurately measure the respiratory cycle of different individuals.

III. PROJECT PROPOSAL

This capstone project aims to utilize Qvar to design and build a device related to respiratory systems on an Android

platform. This project will research and solve the following questions: 1) how to measure and collect data in an accurate manner, 2) how to transfer data between different devices on different operating system, 3) how to sync data and present to users in a short period of time, and 4) how to lower and eliminate the chance of error occurrence under different circumstances.

The research design will be based on either electrodes or a chest strap. Electrodes can be used to measure dissolved oxygen levels in blood. The chest strap would measure a change in pressure or volume around the ribcage. A chest strap involves thorax and abdomen restriction, which forces the subject to breathe at low lung volumes [5].

The procedure of the project research is divided into four steps: 1) Data collection and storage of data, 2) Gather sample and sampling procedure, 3) Build model and analyze data, 4) Apply a Machine Learning model to train and predict the data. While collecting data, the process involves a total of 4 subjects (1 male and 3 females). Data will be stored in the Qvar SD card of a device from an Android mobile device to a computer to plot data. While processing with the data collection, the research will require each subject to sit, stand or walk with a commercial chest strap and electrode system in place. Each

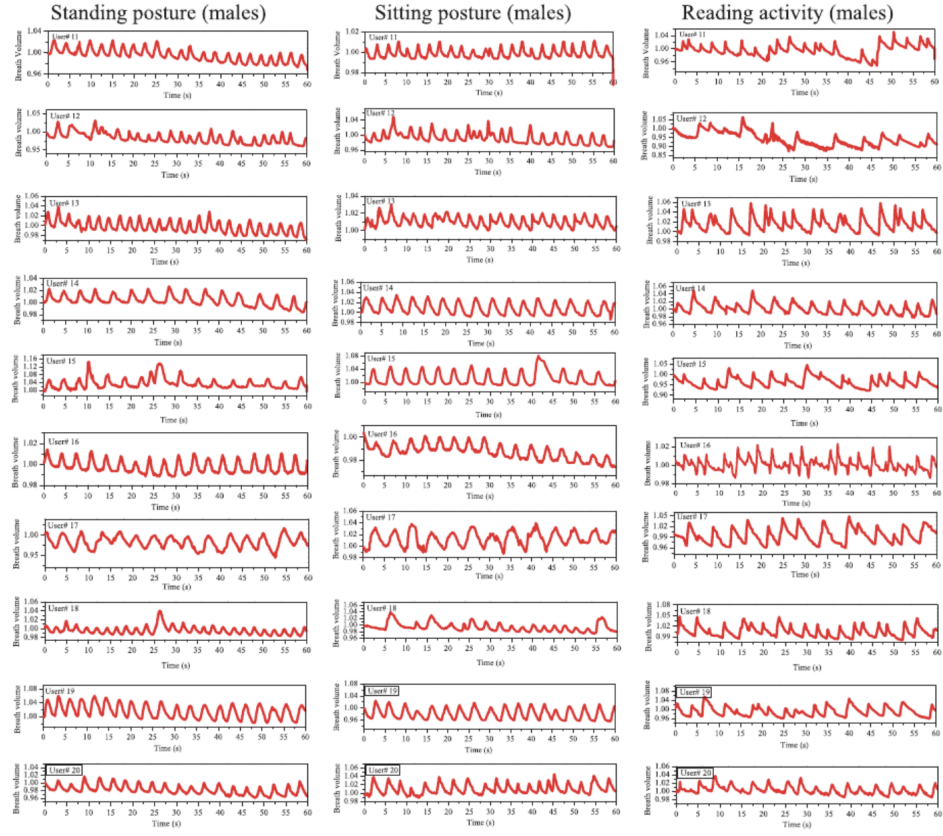


Fig. II.5. Respiration patterns of male users adduced during standing, sitting postures, and reading activities [9]

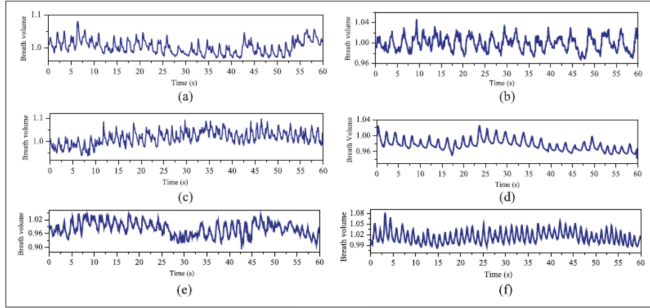


Fig. II.6. Comparison of test patterns under different physical activity conditions: (a) riding a stationary or indoor bike, (b) indoor walking activity respiration pattern, (c) jogging on an elliptical cross trainer, (d) after jogging on an elliptical cross trainer, (e) training on the pec deck machine, and (f) after training on the pec deck machine [9]

subject will continue the process for 60 seconds for each data trial. For consistency and comparison, all baseline data of each subject will be recorded with the NeuLog Neuron Logger Sensors NUL-236 Respiration Monitor Belt Logger Sensor at the same time. Each participant will collect 15 trials of data for each position (sitting, standing, and walking). After importing the data from the SD card to a computer, the team will experiment with Python to analyze and filter the data, and, from there, apply a machine learning model

to predict respiratory rate based on the signals. To determine the model's performance under different circumstances, data will be collected with varying electrode placement, device placement, participants, and clothing. Finally, the Qvar data will be compared to ground truth data for accuracy.

The ethical considerations include the following terms: 1) informed consent for data collection, 2) confidentiality, 3) do no harm, and 4) assessment of only relevant components. The setting and workspace of the research and project will be held in Lab 1762 Boelter Hall, at the University of California - Los Angeles. The limitations of data from this project include a small sample size of 4 subjects, limited age range of 21-23, and lack of gender and ethnicity diversity. All 4 subjects are also healthy. Further limitations of the project include the limited time frame and hardware limitations.

IV. ANALYSIS

A. Data Collection

The team first collected baseline data for each subject to compare with the Qvar data later. Each subject used a NeuLog Respiration Monitor Belt Sensor for collecting sets of data. Each sample consisted of 60 seconds of breathing in each of the three positions studied.

Below, Figures 4.1 to 4.3 show an example of one trial of the normalized pressure ground truth data and the filtered

Qvar data of participant 3's breathing patterns in the sitting, standing, and walking positions. The normalized pressure ground truth data was raw data of breath cycles from the NeuLog device, and the filtered Qvar data was data that was filtered with the HeartPy Python toolkit.

For the sitting position, the Qvar data shown in IV.1 estimates that subject 3 had 6 breaths per minute. As shown in IV.1, the filtered Qvar data (above) matches patterns of the waveforms with the ground truth (below) perfectly.

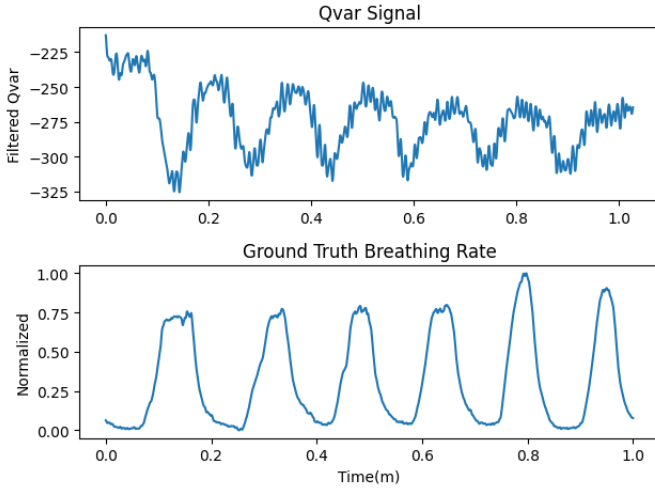


Fig. IV.1. Person 3 Qvar and Ground Truth Sitting Sample

The ground truth standing data in IV.2 shows the participant had around 8 breaths per minute while standing. The participant's breaths were evenly spread throughout the trial. However, in the upper half of IV.2, the filtered Qvar data provided a much noisier signal. The Qvar data for the standing position does not show a respiratory waveform that corresponds with the ground truth waveform.

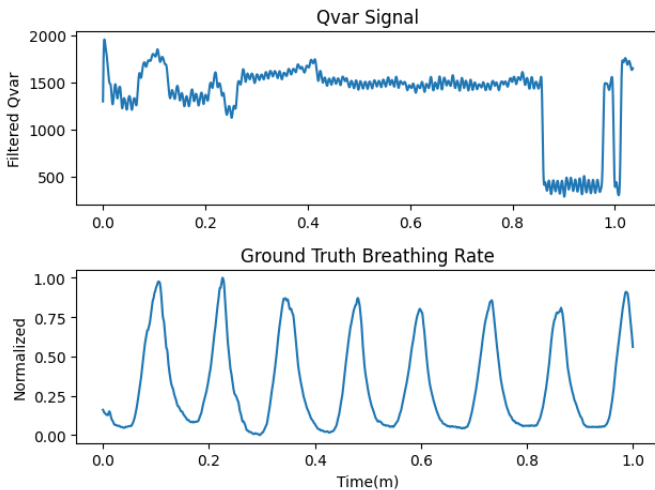


Fig. IV.2. Person 3 Qvar and Ground Truth Standing Sample

The participant had around 10 breaths per minute while walking. However, the ground truth waveform in IV.3 shows

slight differences from the sitting and standing ground truth waveforms. The walking ground truth waveform was noticeably noisier than the sitting and standing ground truth waveforms. The filtered Qvar data performed well and was able to match the number of breaths found in the ground truth waveform since the dark blue curve in the middle of the filtered Qvar waveform also had around 10 breaths.

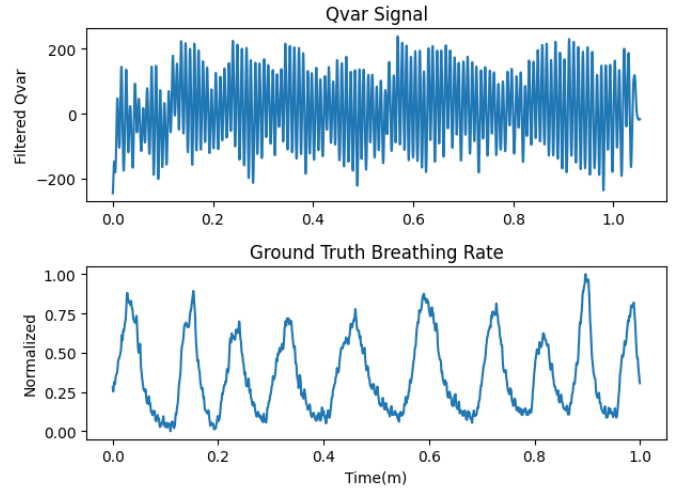


Fig. IV.3. Person 3 Qvar and Ground Truth Walking Sample

Each subject took 15 trials of data in three positions: sitting, standing, and walking. Table 4.1 shows each participant's baseline data of the number of breaths per minute. The experiment analyzed and compared data across positions for accuracy and precision.

Participant 1's breathing data varied in a range from 12 to 14 breaths per minute in the sitting position, 11 to 12 breaths per minute in the standing position, and 10 to 13 breaths per minute in the walking position. The sitting ground truth waveforms had 2 to 3 breaths more per minute than the standing position waveforms, and the standing position waveforms had 1-3 breaths per minute more than the walking position waveforms. Furthermore, the data showed participant 1's breath was slightly affected by positions.

Participant 2's breathing data varied in a range from 30 to 32 breaths per minute in the sitting position, 34 to 36 breaths per minute in the standing position, and 42 to 45 breaths per minute in the walking position. Participant 2 had lower breathing counts while sitting and standing, and a higher breathing counts while walking. The data showed that participant 2's breaths per minute was greatly affected by positions.

Participant 3's breaths varied in a range from 6-7 breaths per minute in the sitting position, 7-8 breaths per minute in the standing position, and 10-11 breaths per minute in the walking position. The participant's sitting ground truth waveforms had 1 to 2 breaths per minute less than the standing ground truth waveforms, and the standing ground truth waveforms had 3-4 less breaths per minute than the walking position. The data

showed that participant 3's breathing counts were slightly affected by positions. Sitting waveforms had the lowest number of breaths, while walking waveforms had the highest number of breaths.

Participant 4's breaths varied in a range from 10 to 11 breaths per minute in the sitting position, 11 to 13 breaths per minute in the standing position, and 12 to 16 breaths per minute in the walking position. The sitting position ground truth waveforms had 1-2 breaths per minute less than the standing position ground truth waveforms, and the standing position ground truth waveforms had 1-3 breaths per minute less than the walking position ground truth waveforms, which mean participant 4's breath was not significantly affected by positions.

As shown in Table 4.1, participants 1, 3, and 4 had similar respiration patterns, except that participant 1 was oppositely proportional with participants 3 and 4. These three participants' breaths per minute were not significantly affected by positions. The breaths per minute of participant 2 varied more significantly across sitting, standing, and walking positions in comparison to participants 1, 3, and 4.

B. Qvar Respiration Data

To collect Qvar Respiration data, the experiment required the following items: two 3M-2238 electrodes, two alligator cable clips, two male-to-female sensor cables, a SensorTile.box PRO, a Qvar sensor board STEVAL\$MKI235AA, a NeuLog Respiration Monitor Belt Sensor with NUL-208 Heart Rate & Pulse Logger Sensor and NUL-236 Respiration Monitor Belt Logger Sensor, and an Android mobile device with ST OEM.box. The NeuLog chest strap and the Qvar board were used to record at the same time to collect ground truth and compare the respiration patterns.

The two electrodes were attached to the participants' torso and disposed once data collection was finished. One electrode was attached to the upper right chest of the participant, and the other was attached to the lower left rib. Keeping two electrodes further from each other helped decrease the occurrence of continual noises. The next step was to connect one end of an alligator clip to an electrode patch and the other end to a male side of a sensor cable. Repeat this same process for the other pair of items.

The procedure of Qvar respiration data collection was divided into seven steps: 1) Pin a Qvar sensor board on a SensorTile.box PRO by the GND and VDD of the box. 2) Connect the two female ends of the sensor cable to QVAR1 and QVAR2 pins on the board. 3) Connect the cable, the alligator clips, and electrode patches based on the previously described process. 4) Put on the NeuLog Belt Sensor and plug it into a computer with the NeuLog application to log .csv data (the waveforms). 5) Turn on a SensorTile.box PRO and connect to the STMicroelectronics Android app STMicroelectronics (ST OEM.box). 6) Set up the log setting to 200Hz output data rate (ODR), click on the box of Enable Qvar, and 60Hz on the notch setting. 7) Log Qvar breathing

data to the SD card inside the SensorTile.box Pro and the ground truth data on the computer.

For analyzing the collected Qvar respiration data, the team experimented initially with HeartPy, a Python heart rate analysis toolkit. This toolkit was utilized as a potential package for analyzing Qvar breathing data as an ECG-like setting. IV.5 shown below represents an example for plotting the sitting data with a filter to reduce the effects of noise. With a cutoff of 2.65 Hz, the HeartPy was able to filter out most of the noise and provide a neat breathing pattern.

Although HeartPy was able to filter out most of the noise, it struggled to produce accurate breathing and heart rates. Because of this, alternative filtering techniques and a machine learning model were utilized to accurately estimate breaths per minute from the Qvar signals. Overall, the process of respiration data collection followed the steps of experiment setup, collection of each participant's data, and analysis of data through filtering and machine learning.

C. Optimizing Parameters For Data Collection

A major issue that was encountered during data collection involved the signal being too noisy to directly obtain respiratory rate values. Throughout the experiments, the aim was to collect respiratory data and use the HeartPy toolkit and other signal processing techniques to obtain respiratory rates, analyzing their accuracy based on the ground truth data. The goal was to identify which setups and parameters would provide the most accurate results. To start out, the SensorTile.box PRO was used with connections on the QVAR1 and QVAR2 pins to two electrodes connected to the upper left and right sides of the chest. Very noisy values with this setup were observed, so different positions of the electrodes were tested to see what would work best. These setups included two electrodes on the upper chest, two on the ribs/abdomen, one on the upper right chest and one on the left ribs/abdomen, one on the upper left chest and one on the right ribs/abdomen, as well as with a singular electrode on the upper chest. It was found that the setup with one electrode on the right chest and one on the left ribs/abdomen worked best, which matched the observations from the research [7].

To confirm that the RA-LL electrode setup would be the most accurate, a setup using the Qvar radar sensor was also tested. The radar sensor was placed roughly 4 inches in front of the chest to measure chest displacement, but exaggerated breathing was required in order to detect peaks from each breath, especially with standing and walking. As shown in IV.6 and IV.7, even with filtering, the resulting data also did not resemble the characteristics of ground truth waveform. Additionally, the setup itself provided greatly varying results across trials due to the need for greater chest movement while breathing.

The lack of consistency with this setup confirmed that electrodes would be the best approach for data collection. After obtaining the optimum electrode placement (similar to the ECG), the data still had significant noise levels. To try and improve the signal-to-noise ratio, changes were implemented

Fig. IV.4. Baseline Data

| Baseline Data: Number of Breaths Per Minute | | | | | | | | | | | | | |
|---|----------|----------|---------|----------|----------|---------|----------|----------|---------|----------|----------|---------|--|
| | Person 1 | | | Person 2 | | | Person 3 | | | Person 4 | | | |
| Trial # | Sitting | Standing | Walking | |
| 1 | 14 | 12 | 11 | 33 | 34 | 43 | 6 | 8 | 10 | 10 | 13 | 16 | |
| 2 | 13 | 12 | 13 | 30 | 34 | 45 | 6 | 8 | 10 | 11 | 13 | 14 | |
| 3 | 13 | 12 | 12 | 32 | 34 | 44 | 6 | 8 | 10 | 11 | 13 | 14 | |
| 4 | 13 | 12 | 12 | 31 | 35 | 45 | 6 | 8 | 10 | 10 | 11 | 15 | |
| 5 | 13 | 11 | 11 | 31 | 35 | 43 | 6 | 8 | 10 | 10 | 13 | 15 | |
| 6 | 14 | 12 | 13 | 32 | 34 | 42 | 7 | 8 | 10 | 10 | 11 | 14 | |
| 7 | 13 | 12 | 11 | 32 | 35 | 42 | 7 | 8 | 10 | 11 | 13 | 14 | |
| 8 | 13 | 12 | 10 | 31 | 34 | 45 | 6 | 8 | 11 | 10 | 13 | 16 | |
| 9 | 13 | 12 | 11 | 31 | 37 | 42 | 7 | 8 | 10 | 11 | 13 | 16 | |
| 10 | 13 | 12 | 11 | 31 | 35 | 42 | 6 | 8 | 10 | 11 | 11 | 13 | |
| 11 | 12 | 12 | 11 | 31 | 32 | 44 | 6 | 7 | 10 | 11 | 11 | 12 | |
| 12 | 12 | 12 | 11 | 31 | 35 | 43 | 6 | 8 | 11 | 10 | 12 | 14 | |
| 13 | 13 | 11 | 11 | 31 | 34 | 45 | 7 | 8 | 10 | 10 | 13 | 14 | |
| 14 | 13 | 12 | 11 | 32 | 34 | 44 | 7 | 8 | 11 | 10 | 11 | 13 | |
| 15 | 13 | 11 | 12 | 32 | 36 | 45 | 6 | 8 | 11 | 11 | 12 | 13 | |
| 16 | | | | | | | 6 | 8 | 10 | 11 | 12 | | |
| 17 | | | | | | | 7 | 8 | 10 | | | | |
| 18 | | | | | | | 6 | 8 | 10 | | | | |
| 19 | | | | | | | 6 | 8 | 10 | | | | |
| 20 | | | | | | | | | | | | | |

```
def sitting_plot(df):
    data = df['QVAR [LSB]'].to_numpy()
    sampling_rate = 200.0
    #filtered = hp.remove_baseline_wander(data,sample_rate = sampling_rate, cutoff = 2.7)
    filtered = hp.filter_signal(data, cutoff = 2.65, sample_rate = sampling_rate, order = 3, filtertype='lowpass')
    #filtered = hp.hampel_correcter(data,sample_rate = sampling_rate)
    #time = np.linspace(0,filtered.shape[0]*(1/sampling_rate),filtered.shape[0])
    time = df['Timestamp [us]']
    time = time/60000000
    #df.plot(x='Timestamp [us]', y='QVAR [LSB]')
    plt.plot(time,filtered)
    plt.xlabel('Time(m)')
    plt.ylabel('Filtered')
```

Fig. IV.5. Example of HeartPy with A Filter for A Sitting Plot

in the hardware setup. Different SensorTile.box PRO boards with the ST OEM.box app were experimented with. Furthermore, attempts were made to utilize the STENG1AX with the ProfiMEMS using Unico. However, as shown in IV.8 and IV.9, similar noisy results were achieved. In another attempt to reduce noise, shorter wires were used and shielding the wires was attempted using aluminum foil. Contact points were also insulated using electrical tape, but the waveforms still showed similar noise levels, indicating that further experimentation was needed.

The next step was to make sure that the Qvar pin connections were working as intended and were collecting interpretable data. To rule out the SensorTile.box PRO as the culprit for noise, tests were conducted with the Qvar touch sensor.

On looking at the log file, it could be seen that there were spikes corresponding to the taps, indicating that the Qvar pins were collecting data as intended. This likely meant that the noise was a result of this study's setup. To test that hypothesis, noise creation was attempted, where wires were connected to the Qvar pins and random noise patterns were generated to ensure data was being recorded.

When tapping the wires on the table, spikes in the Qvar values corresponding to the taps were seen, as shown in IV.10. This showed that the noise was primarily in the electrode setup and that the signal-to-noise ratio obtained directly from data collection was very high. Then, the focus became identifying the best possible settings for the output data rate (ODR) on the app. The goal was to find a balance between obtaining

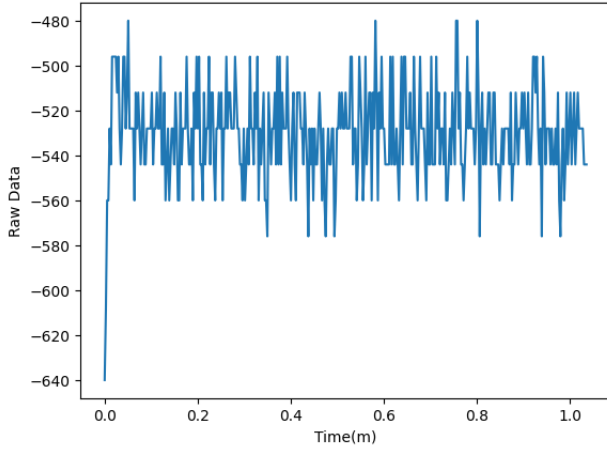


Fig. IV.6. Radar Attempt Raw Data Sample

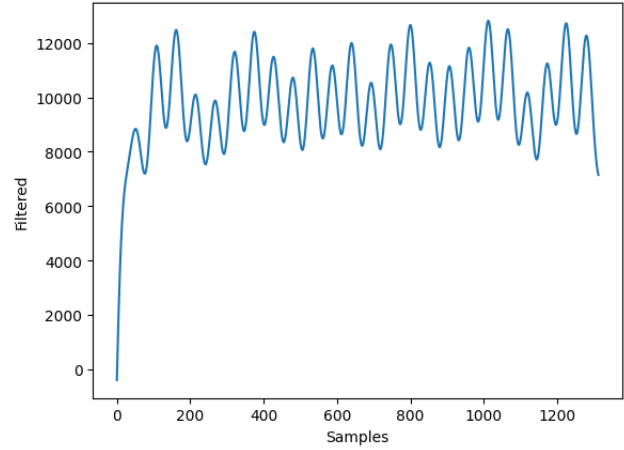


Fig. IV.9. ProfiMEMS Sensor Person 2 Filtered Data Sample: 0.18 Breathing Rate in HeartPy

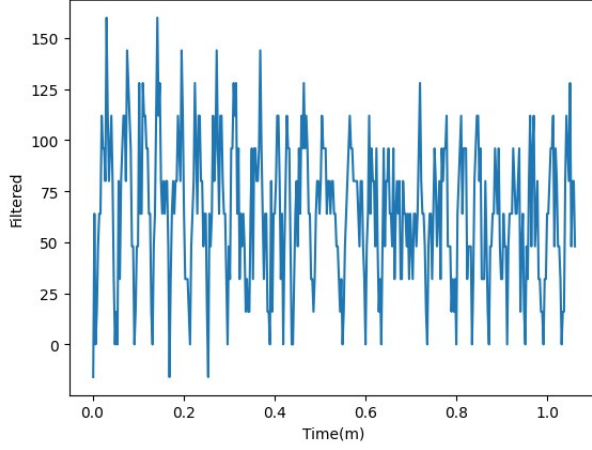


Fig. IV.7. Radar Attempt Filtered Data Sample

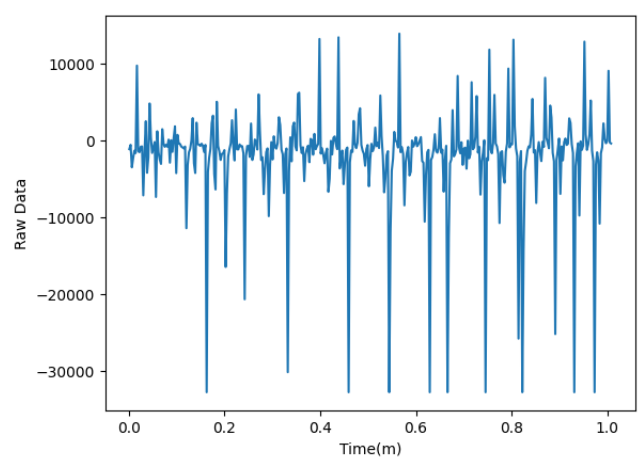


Fig. IV.10. Noise Creation Raw Data

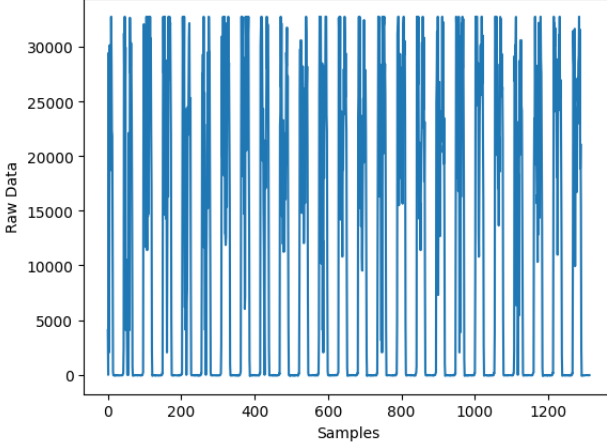


Fig. IV.8. ProfiMEMS Sensor Person 2 Raw Data Sample: 0.18 Breathing Rate in HeartPy

as many samples as needed while ensuring that the signal could be processed and interpreted for breathing characteristics

(an issue with the much larger ODRs). ODRs of 6 Hz, 12.5 Hz, 25 Hz, and 200 Hz were tested and samples of Qvar data over a period of one minute for sitting, breathing, and walking positions were collected. The results are shown in IV.11, IV.12, IV.13, IV.14, IV.15, IV.16, IV.17, and IV.18. The three postures still saw similar outcomes, with the 200 Hz ODR providing the most information. These signals were still able to be processed and interpreted after data collection with respiratory rate characteristics closer to ground truth, so 200 Hz ODR was used as the standard ODR for the trials.

It should be noted that the Qvar waveform itself should not match the shape of the ground truth respiratory waveform as the data collection processes involved two completely different methods of data collection: pressure for baseline and electrostatic for the Qvar.

Once a standardized ODR was selected, other settings on the app such as notch, Z_{in} , and gain were experimented with. There was not much variation with the Z_{in} and gain, so these settings were kept at the default settings on the app. However, as shown in IV.19, IV.20, IV.21, and IV.22, applying the 50

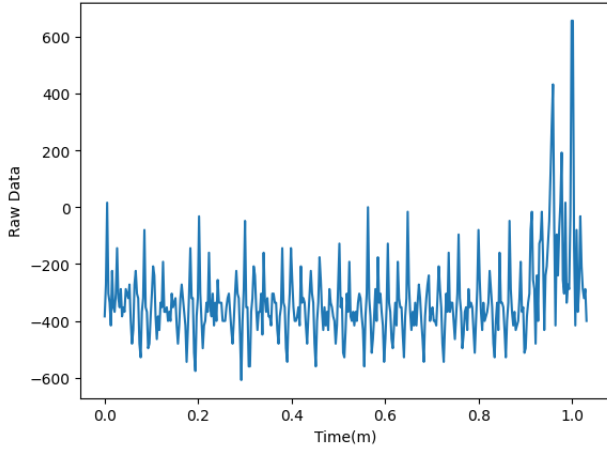


Fig. IV.11. Raw 6 ODR Sitting Data Sample: NaN Breathing Rate in HeartPy

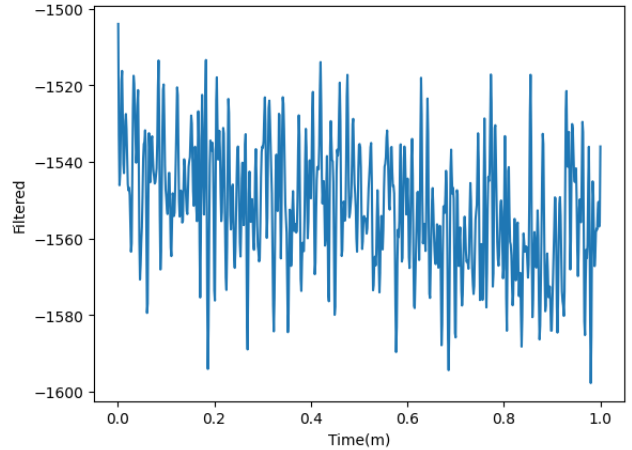


Fig. IV.14. Filtered 12.5 ODR Sitting Data Sample: 0.38 Breathing Rate in HeartPy

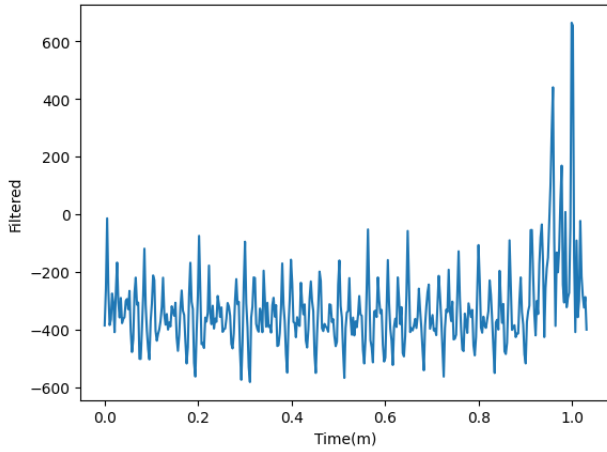


Fig. IV.12. Filtered 6 ODR Sitting Data Sample: 0.33 Breathing Rate in HeartPy

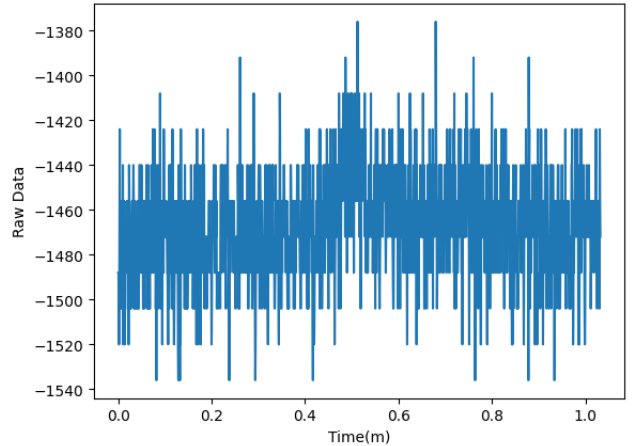


Fig. IV.15. Raw 25 ODR Sitting Data Sample: 0.23 Breathing Rate in HeartPy

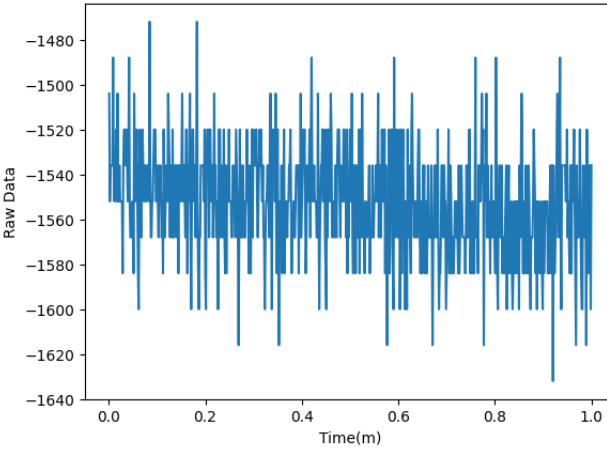


Fig. IV.13. Raw 12.5 ODR Sitting Data Sample: 0.2 Breathing Rate in HeartPy

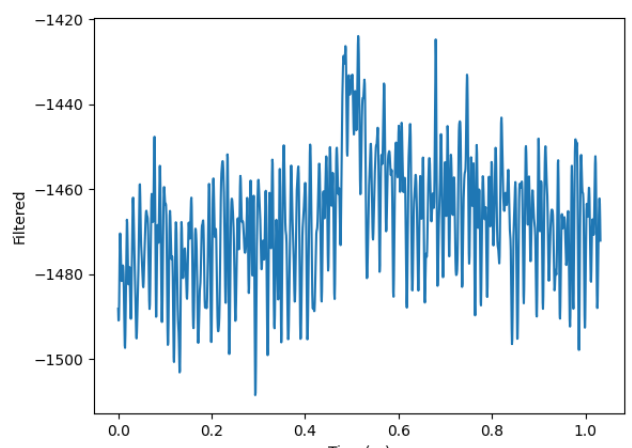


Fig. IV.16. Filtered 25 ODR Sitting Data Sample: 0.14 Breathing Rate in HeartPy

Hz and 60 Hz filters did produce slightly different waveforms, with the 60 Hz filter providing characteristics for respiratory

rate more similar to the ground truth waveforms. As a result,

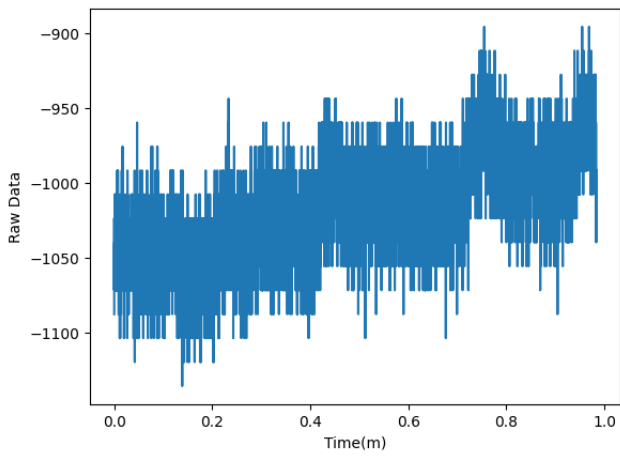


Fig. IV.17. Raw 200 ODR Sitting Data Sample: 0.37 Breathing Rate in HeartPy

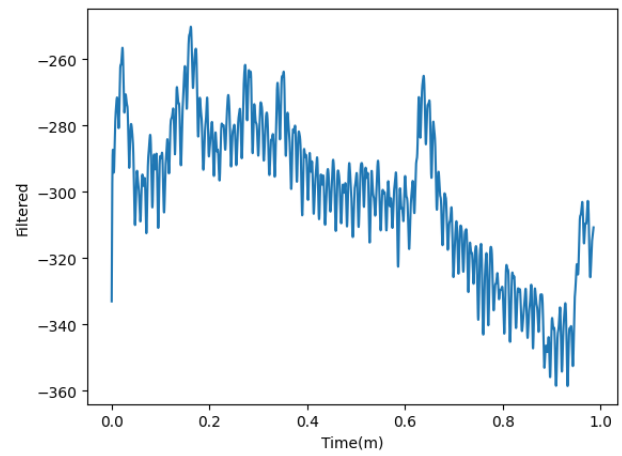


Fig. IV.20. Filtered 50 Hz Notch Sitting Data Sample: 0.24 Breathing Rate in HeartPy

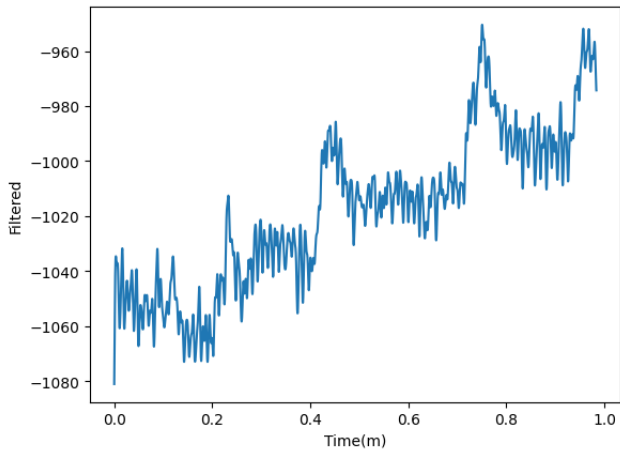


Fig. IV.18. Filtered 200 ODR Sitting Data Sample: 0.20 Breathing Rate in HeartPy

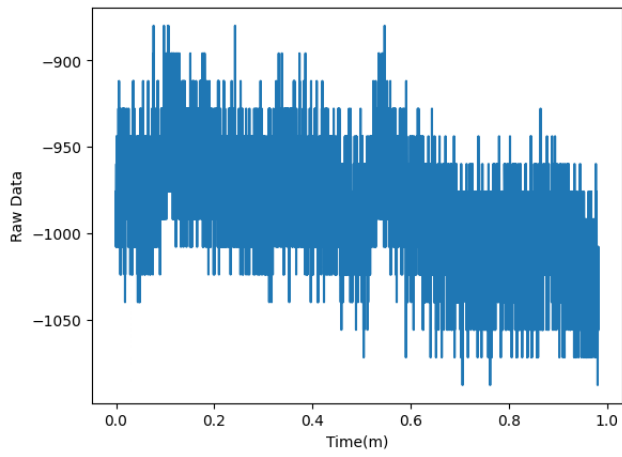


Fig. IV.21. Raw 60 Hz Notch Sitting Data Sample: 0.20 Breathing Rate in HeartPy

this study used a 60 Hz notch filter.

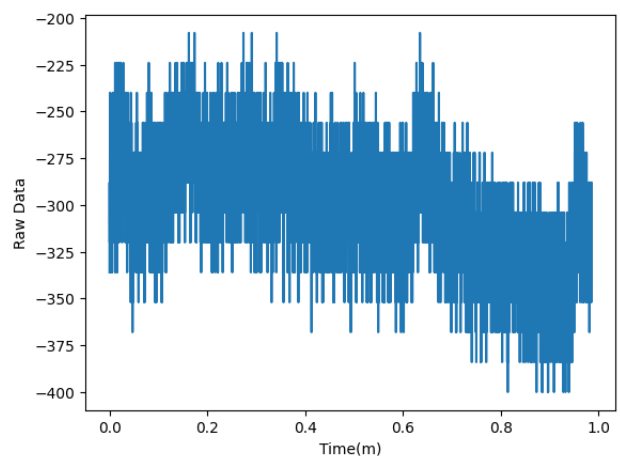


Fig. IV.19. Raw 50 Hz Notch Sitting Data Sample: 0.28 Breathing Rate in HeartPy

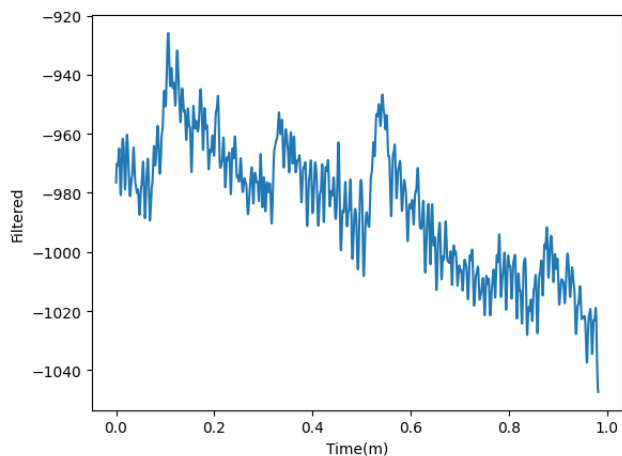


Fig. IV.22. Filtered 60 Hz Notch Sitting Data Sample: 0.16 Breathing Rate in HeartPy

Overall, even with these changes, the Qvar signal obtained from direct data collection was still noisy. Signal processing techniques including low pass filters, high pass filters, notch filters, as well as combinations of different filters were tested. The remove baseline wander filter in the HeartPy toolkit was also tested but determined not to be the best fit. It was found that enabling the low pass filter using the HeartPy toolkit proved to reduce noise the most (the filtered signals above follow this method). However, the Qvar signal still had significant noise even after signal processing and the respiratory rate was still not interpretable. The next approach was to build a machine learning model to overcome the limitations of signal processing with the hardware setup.

D. Machine Learning Approach

After attempting to produce the breathing rate directly through filtering the raw data by minimizing noise using the approaches discussed above and not having much success, it was decided to use a machine learning approach. Fifteen to twenty samples of data were taken from each of the four participants for sitting, standing, and walking. Each sample consisted of a minute of data in which the participant was breathing normally in one of the three positions. The samples were taken at 200 ODR, with a 60 Hz notch filter to reject the power line noise with the Qvar sensor in the SensorTile.box PRO. The ground truth was taken with the NeuLog Neuron Logger Sensors NUL-236 Respiration Monitor Belt Logger Sensor simultaneously.

These samples were then used to generate multiple machine learning models using different sets of data. STMicroelectronics provided access to Unico GUI which has a built-in machine learning feature that allows input of datasets and customization of certain features and settings. It then produced a decision tree for the given data and the accuracy of that decision tree. Unico uses a variation of the J48 tree training algorithm, which is an implementation of the C4.5 algorithm. The C4.5 algorithm is a modification of the ID3 algorithm. It uses the information gain to determine which attributes to utilize to split the data [6]. It uses an 80% and 20% split in data as training and validation data, respectively.

In order to use this function, the data had to be preprocessed. Because the Unico GUI was set to process accelerometer data, the Qvar data was labeled as accelerometer data. The Qvar data was fed in as if it was accelerometer data to allow Unico to classify it correctly. The raw data was in the format as shown in IV.23 where the column of interest is ‘Qvar [LSB]’. This was then processed into the format in IV.24 into the column ‘A_X [mg]’ to allow the Unico GUI to process it.

Because the Unico GUI was unable to produce a regression model, the next step was determining the classification labels. It was decided to use breathing rate ranges. The data was split into buckets of five starting at 6 breaths per minute up to 45 breaths per minute, yielding eight buckets. For buckets in which there was no data, one data set full of zeros was introduced as a placeholder to create the label. The data was put into the Unico GUI as seen in IV.25, where the data is

| | Timestamp [us] | A_X [LSB] | A_Y [LSB] | A_Z [LSB] | A_X [mg] | A_Y [mg] | A_Z [mg] | QVAR [LSB] |
|-------|----------------|-----------|-----------|-----------|----------|----------|----------|------------|
| 0 | 4312 | -368 | 288 | 16224 | -22.448 | 17.568 | 989.664 | -1136 |
| 1 | 9315 | -336 | 336 | 16224 | -20.496 | 20.496 | 989.664 | -1136 |
| 2 | 14318 | -368 | 336 | 16192 | -22.448 | 20.496 | 987.712 | -1120 |
| 3 | 19318 | -368 | 384 | 16240 | -22.448 | 23.424 | 990.640 | -1136 |
| 4 | 24320 | -352 | 384 | 16256 | -21.472 | 23.424 | 991.616 | -1120 |
| ... | ... | ... | ... | ... | ... | ... | ... | ... |
| 11941 | 59734920 | -320 | 432 | 16180 | -19.520 | 26.352 | 985.760 | -1168 |
| 11942 | 59739922 | -352 | 320 | 16256 | -21.472 | 19.520 | 991.616 | -1184 |
| 11943 | 59744923 | -352 | 368 | 16192 | -21.472 | 22.448 | 987.712 | -1184 |
| 11944 | 59749925 | -368 | 320 | 16176 | -22.448 | 19.520 | 986.736 | -1184 |
| 11945 | 59754927 | -352 | 368 | 16224 | -21.472 | 22.448 | 989.664 | -1168 |

Fig. IV.23. Raw Data Table Format

| | A_X [mg] | A_Y [mg] | A_Z [mg] |
|-------|----------|----------|----------|
| 0 | -1088 | 0 | 0 |
| 1 | -1024 | 0 | 0 |
| 2 | -1088 | 0 | 0 |
| 3 | -1072 | 0 | 0 |
| 4 | -1056 | 0 | 0 |
| ... | ... | ... | ... |
| 11798 | -1040 | 0 | 0 |
| 11799 | -1008 | 0 | 0 |
| 11800 | -992 | 0 | 0 |
| 11801 | -992 | 0 | 0 |
| 11802 | -992 | 0 | 0 |

Fig. IV.24. Preprocessed Data Table Format

chosen by clicking browse. Then, the label is typed into ‘Set Class (Label)’ and the data is loaded to be used to generate a model.

In order to fine tune the model, the settings were modified. The models were tested with different windows (samples provided), nodes, and enabled filters. Windows of 52, 105, and 255 and nodes of 30, 50, and 80 were tested. The model was also tested with no filter and with an HP ACC filter. The machine learning core ODR was set to 100 Hz. This was the sampling rate of the data divided by the number of channels used. The Qvar had two channels, but took a differential, giving only one column of data. The accelerometer ODR was set at 200 Hz to match the settings used when taking samples. All features corresponding to the acceleration in X, where the column of Qvar data is located, are enabled for the machine learning core to choose from. After testing multiple times, the settings that provided the most accurate models were found to be a window of 255 with 30 nodes and the differential filter. The differential filter limited the maximum nodes to 37, hence why the nodes used ended up being 30. The confidence factor was set to 0.9. These settings in the Unico GUI are shown in

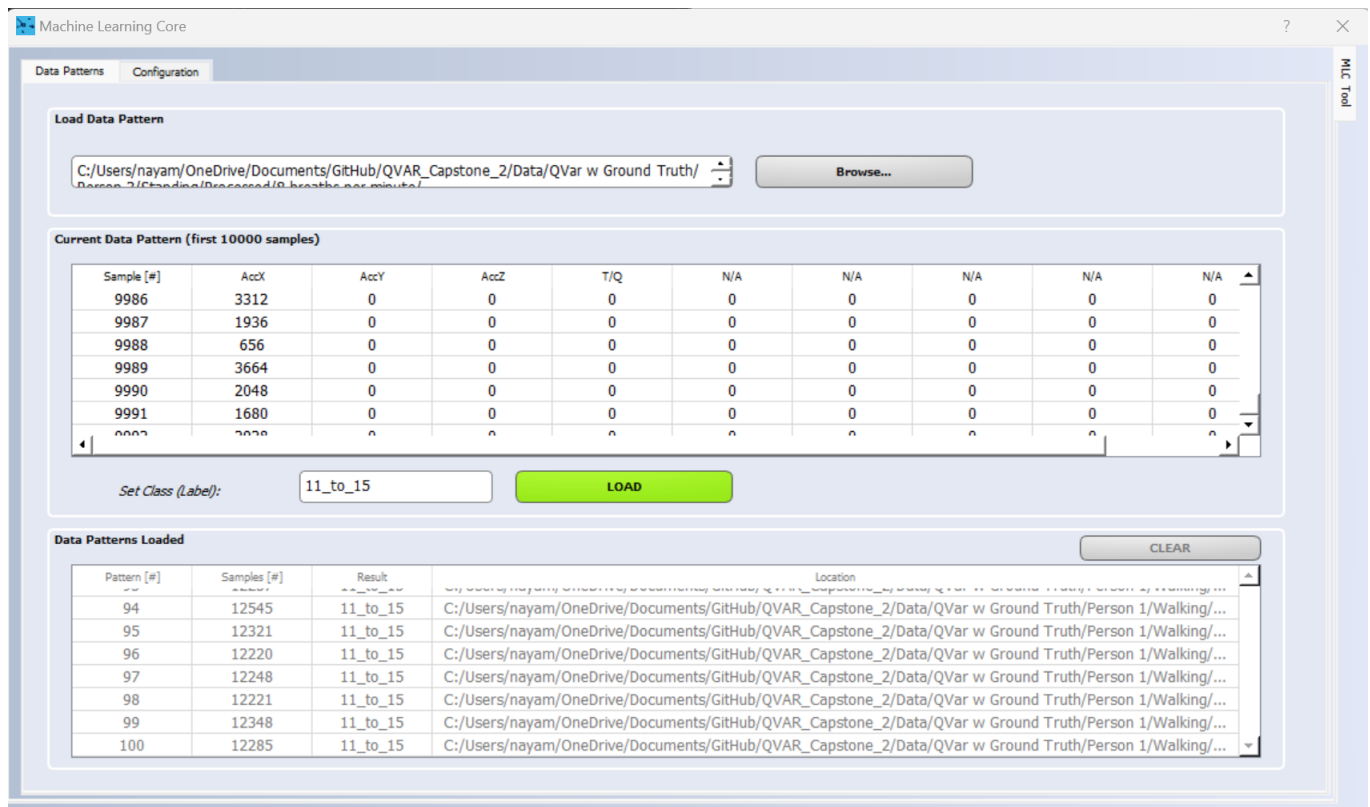


Fig. IV.25. Unico GUI Data Loading

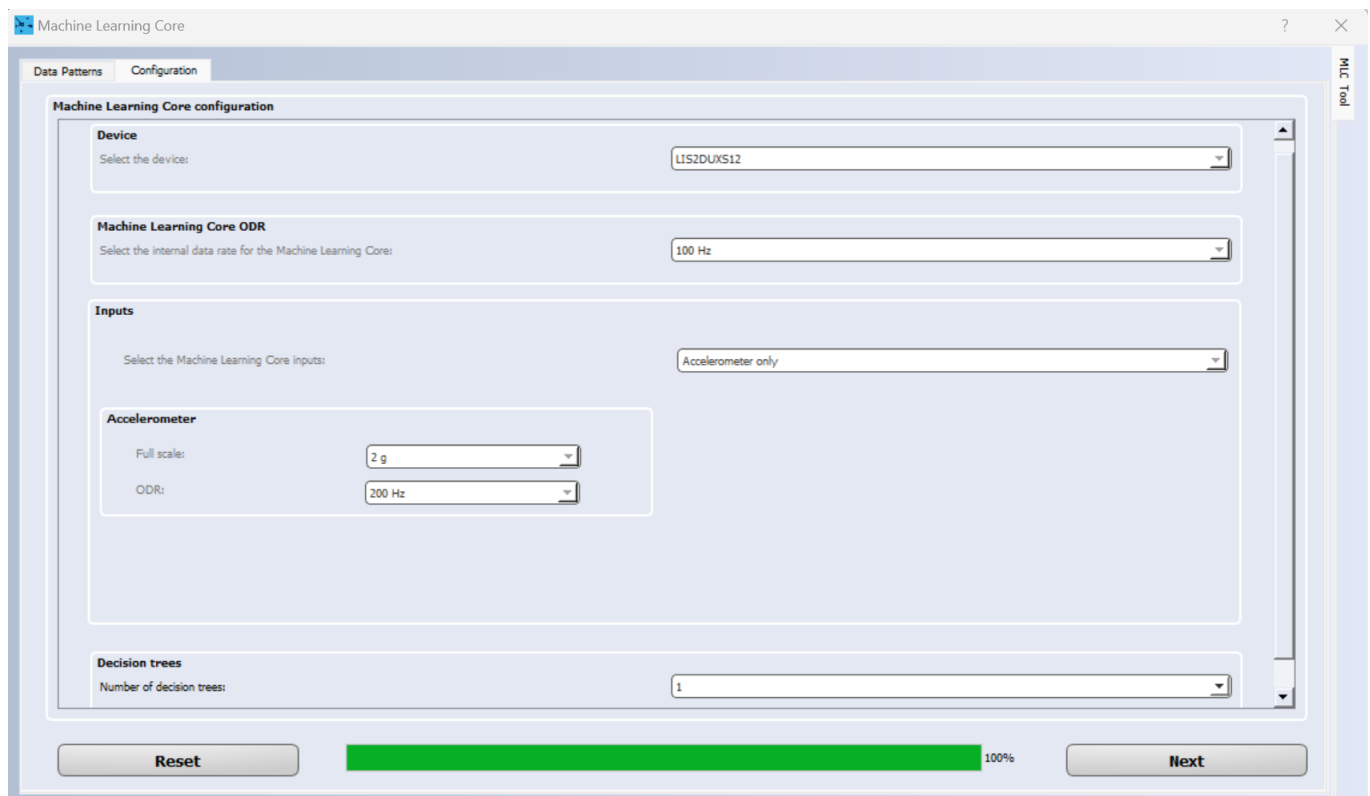


Fig. IV.26. Unico GUI Configuration Settings

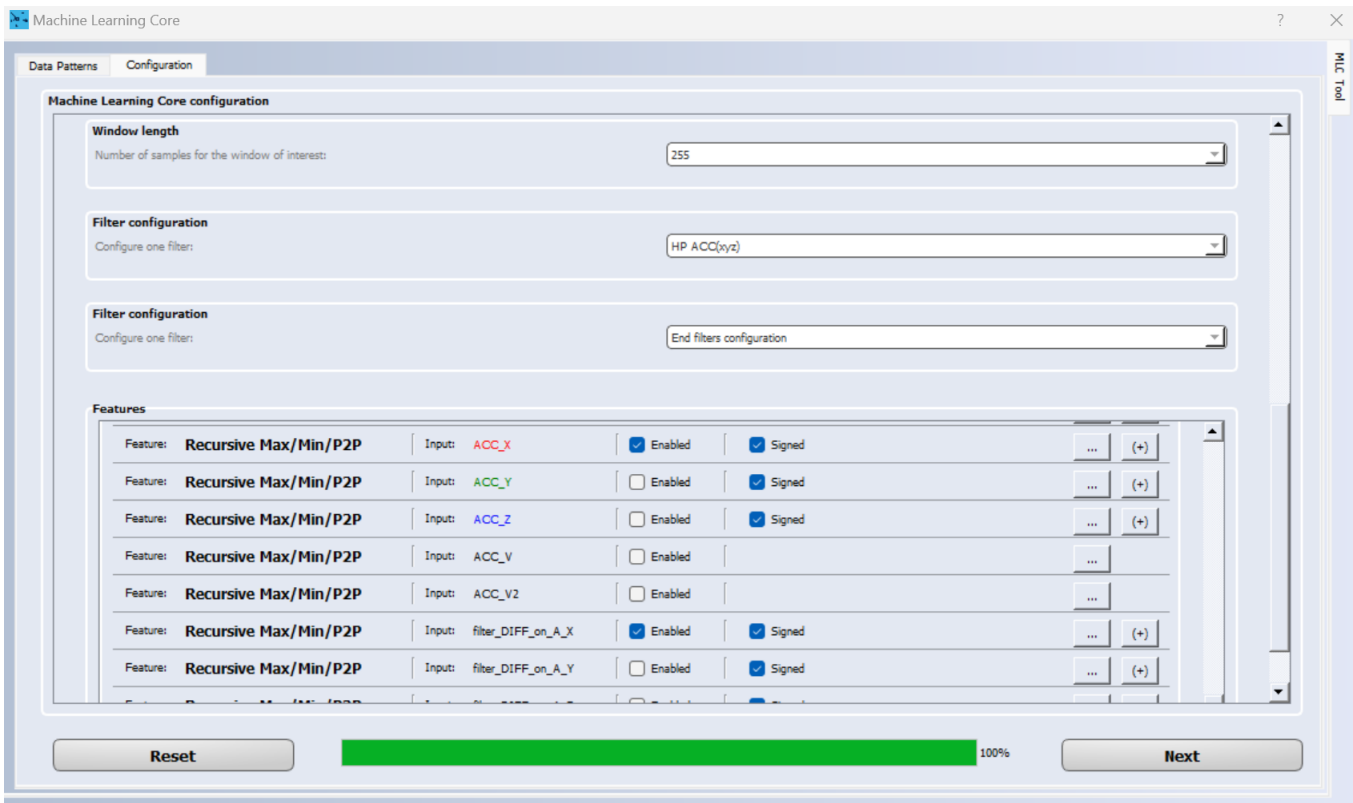


Fig. IV.27. Unico GUI Filter Configuration and Feature Enabling

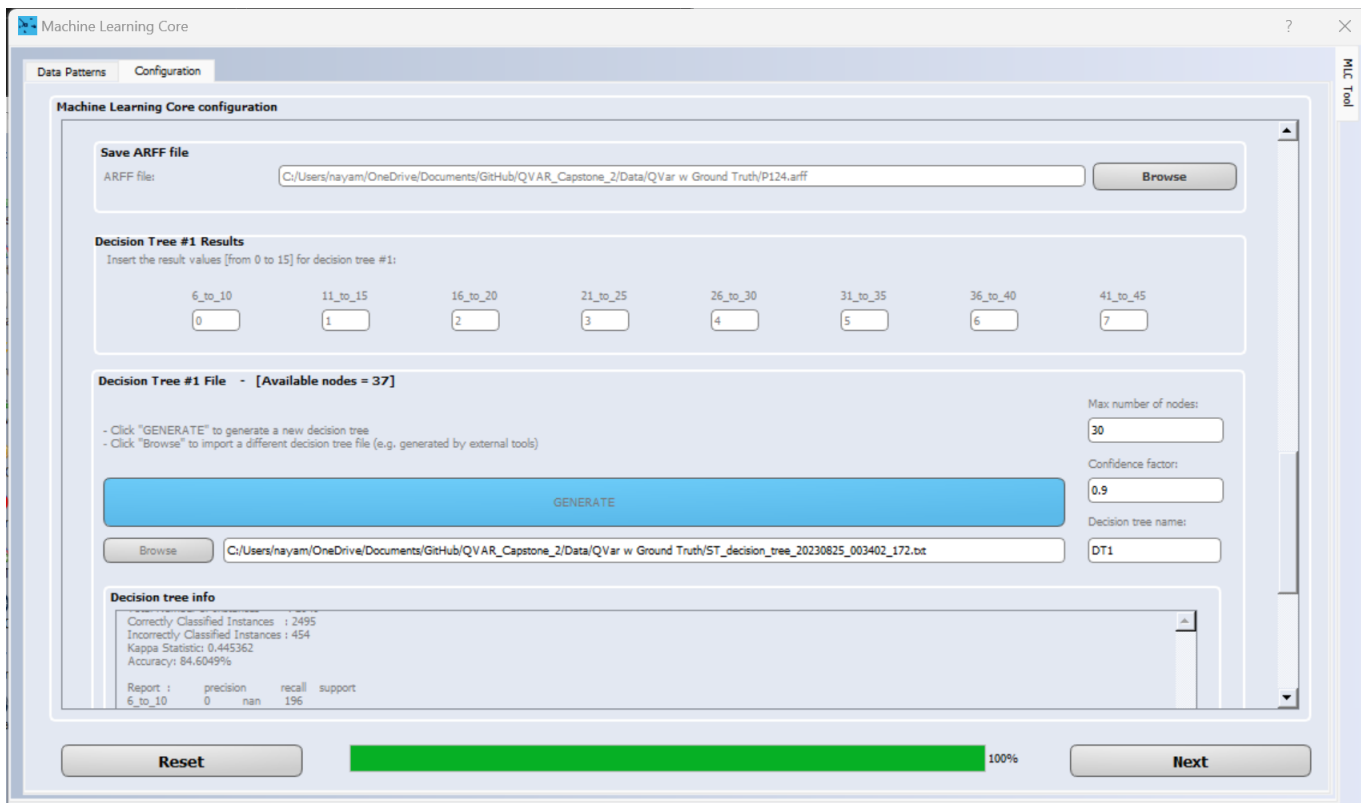


Fig. IV.28. Unico GUI Decision Tree Configuration

```

F1_MEAN_on_ACC_X <= 0.0266154
| F5_ENERGY_on_ACC_X <= 14.3733
| | F21_MIN_on_ACC_X <= -0.23999
| | | F11_PositiveZeroCross_on_ACC_X <= 122
| | | | F5_ENERGY_on_ACC_X <= 4.02734
| | | | | F1_MEAN_on_ACC_X <= -0.0947876: 31_to_35 (16.0)
| | | | | F1_MEAN_on_ACC_X > -0.0947876: 11_to_15 (5.0)
| | | | F5_ENERGY_on_ACC_X > 4.02734
| | | | | F15_PeakDet_on_ACC_X <= 172: 6_to_10 (72.0)
| | | | | F15_PeakDet_on_ACC_X > 172
| | | | | | F30_RECURSIVE_FEATURE_RMS_on_filter_DIFF_on_A_X <= 0.0714427: 31_to_35 (4.0)
| | | | | | F30_RECURSIVE_FEATURE_RMS_on_filter_DIFF_on_A_X > 0.0714427: 6_to_10 (4.0)
| | | | F11_PositiveZeroCross_on_ACC_X > 122
| | | | | F5_ENERGY_on_ACC_X <= 11.3211: 31_to_35 (212.0)
| | | | | F5_ENERGY_on_ACC_X > 11.3211
| | | | | | F9_ZeroCross_on_ACC_X <= 290
| | | | | | | F9_ZeroCross_on_ACC_X <= 270: 6_to_10 (10.0)
| | | | | | | F9_ZeroCross_on_ACC_X > 270: 26_to_30 (5.0)
| | | | | F9_ZeroCross_on_ACC_X > 290
| | | | | | F1_MEAN_on_ACC_X <= -0.0540771: 26_to_30 (2.0)
| | | | | | F1_MEAN_on_ACC_X > -0.0540771
| | | | | | | F3_VAR_on_ACC_X <= 0.0523987: 31_to_35 (48.0)
| | | | | | | F3_VAR_on_ACC_X > 0.0523987: 26_to_30 (1.0)
F21_MIN_on_ACC_X > -0.23999
| F5_ENERGY_on_ACC_X <= 1.29923
| | F23_MAX_on_ACC_X <= 0.0479736: 31_to_35 (275.0/50.0)
| | F23_MAX_on_ACC_X > 0.0479736
| | | F1_MEAN_on_ACC_X <= -0.0471497
| | | | F3_VAR_on_ACC_X <= 0.0013752: 36_to_40 (2.0)
| | | | F3_VAR_on_ACC_X > 0.0013752: 41_to_45 (22.0)
| | | F1_MEAN_on_ACC_X > -0.0471497
| | | | F9_ZeroCross_on_ACC_X <= 210
| | | | | F1_MEAN_on_ACC_X <= -0.0114517
| | | | | | F1_MEAN_on_ACC_X <= -0.0446167: 41_to_45 (3.0)
| | | | | | F1_MEAN_on_ACC_X > -0.0446167: 6_to_10 (1.0)
| | | | | | F1_MEAN_on_ACC_X > -0.0114517: 11_to_15 (8.0)
| | | | F9_ZeroCross_on_ACC_X > 210: 31_to_35 (12.0)
| F5_ENERGY_on_ACC_X > 1.29923: 41_to_45 (284.0/31.0)
F5_ENERGY_on_ACC_X > 14.3733
| F16_PeakDet_on_filter_DIFF_on_A_X <= 196
| | F1_MEAN_on_ACC_X <= -12.96: 11_to_15 (1.0)
| | F1_MEAN_on_ACC_X > -12.96: 6_to_10 (489.0)
F16_PeakDet_on_filter_DIFF_on_A_X > 196
| F4_VAR_on_filter_DIFF_on_A_X <= 0.0325623
| | F1_MEAN_on_ACC_X <= -0.0827026: 6_to_10 (1.0)
| | F1_MEAN_on_ACC_X > -0.0827026
| | | F1_MEAN_on_ACC_X <= -0.0745239: 26_to_30 (1.0)
| | | F1_MEAN_on_ACC_X > -0.0745239: 11_to_15 (1.0)
| | F4_VAR_on_filter_DIFF_on_A_X > 0.0325623: 31_to_35 (3.0)
F1_MEAN_on_ACC_X > 0.0266154
| F22_MIN_on_filter_DIFF_on_A_X <= -0.376022: 6_to_10 (761.0/575.0)
| F22_MIN_on_filter_DIFF_on_A_X > -0.376022: 11_to_15 (1262.0/47.0)

Number of Leaves : 27
Size of the tree : 53

```

Fig. IV.29. Decision Tree for All Data

IV.26, IV.27, and IV.28.

The first model to look at was with all of the data and participants. This resulted in an accuracy rate of 83.29%. The decision tree and decision tree statistics can be seen in IV.29, and IV.30.

It was then decided that all combinations of three out of the four participants should be modeled to analyze the differences in order to discern if there were any biases in the model. The confusion matrices and accuracy percentages for the four combinations of three participants each can be seen below in IV.31, IV.32, IV.33 and IV.34. The full decision trees and statistics can be found in the appendix. As shown, the model with the data of participants 1, 2, and 3 resulted in an accuracy of 91.72%. The model with the data of participants 1, 2, and 4 had an accuracy of 84.60%. The model with the data of participants 2, 3, and 4 had an accuracy of 67.69%, and the model with the data of participants 1, 3, and 4 had an accuracy

of 79.26%. It can be seen that the models with the data of just participants 1, 2, and 3 and participants 2, 3, and 4, are relatively far in accuracy from the model with all the data (83.29%). The difference in accuracy may be accounted for in the fact that participant 2's breathing rates were much higher than that of the other participants. Participants 1, 3, and 4 had breathing ranges between that of 6 to 16 breaths per minute across sitting, standing, and walking while participant 2's breathing ranged between 30 and 45 which was a much larger range and much higher. This skewed the data, and also meant that models that were quite accurate for other participants may not have worked quite as well on participant 2's data. Additionally, when participant 1 and 4's data was modeled together the majority of data was bucketed in the 11 to 15 breaths per minute bucket which means the model is more inclined to put data in that region in those instances.

```

class:
=> 6_to_10, 11_to_15, 16_to_20, 21_to_25, 26_to_30, 31_to_35, 36_to_40, 41_to_45,
features:
=> F1_MEAN_on_ACC_X, F2_MEAN_on_filter_DIFF_on_A_X, F3_VAR_on_ACC_X, F4_VAR_on_filter_DIFF_on_A_X, F5_ENERGY_on_ACC_X, F6
 ENERGY_on_filter_DIFF_on_A_X, F7_PeakToPeak_on_ACC_X, F8_PeakToPeak_on_filter_DIFF_on_A_X, F9_ZeroCross_on_ACC_X, F10
 ZeroCross_on_filter_DIFF_on_A_X, F11_PositiveZeroCross_on_ACC_X, F12_PositiveZeroCross_on_filter_DIFF_on_A_X, F13
 NegativeZeroCross_on_ACC_X, F14_NegativeZeroCross_on_filter_DIFF_on_A_X, F15_PeakDet_on_ACC_X, F16_PeakDet_on_filter_DIFF_on_A_X, F17
 PosPeakDet_on_ACC_X, F18_PosPeakDet_on_filter_DIFF_on_A_X, F19_NegPeakDet_on_ACC_X, F20_NegPeakDet_on_filter_DIFF_on_A_X, F21
 MIN_on_ACC_X, F22_MIN_on_filter_DIFF_on_A_X, F23_MAX_on_ACC_X, F24_MAX_on_filter_DIFF_on_A_X, F25_RECURSIVE_FEATURE_MEAN_on_ACC_X, F26
 RECURSIVE_FEATURE_VAR_on_ACC_X, F27_RECURSIVE_FEATURE_RMS_on_ACC_X, F28_RECURSIVE_FEATURE_MEAN_on_filter_DIFF_on_A_X, F29
 RECURSIVE_FEATURE_VAR_on_filter_DIFF_on_A_X, F30_RECURSIVE_FEATURE_RMS_on_filter_DIFF_on_A_X, F31_RECURSIVE_FEATURE_MAX_on_ACC_X, F32
 RECURSIVE_FEATURE_MIN_on_ACC_X, F33_RECURSIVE_FEATURE_PKPK_on_ACC_X, F34_RECURSIVE_FEATURE_MAX_on_filter_DIFF_on_A_X, F35
 RECURSIVE_FEATURE_MIN_on_filter_DIFF_on_A_X, F36_RECURSIVE_FEATURE_PKPK_on_filter_DIFF_on_A_X,
RECURSIVE_FEATURE_MIN_on_filter_DIFF_on_A_X, F36_RECURSIVE_FEATURE_PKPK_on_filter_DIFF_on_A_X, F36_RECURSIVE_FEATURE_PKPK_on_filter_DIFF_on_A_X, F36

Mean absolute error      0.832205
Root mean squared error 0.833017
===== Whole data training with Confidence Factor: 0.9 =====

===== Confusion Matrix =====
          6_to_10      11_to_15      16_to_20      21_to_25      26_to_30      31_to_35      36_to_40      41_to_45
<- classified as
6_to_10      1338      25      0      0      0      0      0      4
11_to_15      508      1277      0      0      0      0      0      0
16_to_20      44      22      0      0      0      0      0      0
21_to_25      0      0      0      0      0      0      0      0
26_to_30      13      0      0      0      9      0      0      0
31_to_35      10      0      0      0      0      570      0      16
36_to_40      0      0      0      0      0      30      2      11
41_to_45      0      0      0      0      0      20      0      309

Total Number of Instances      : 4208
Correctly Classified Instances : 3505
Incorrectly Classified Instances : 703
Kappa Statistic: 0.308352
Accuracy: 83.2937%

Report :      precision      recall      support
6_to_10      0.979      0.699      1367
11_to_15      0.715      0.965      1785
16_to_20      0      nan      66
21_to_25      nan      nan      0
26_to_30      0.409      1      22
31_to_35      0.956      0.919      596
36_to_40      0.0465      1      43
41_to_45      0.939      0.909      329

avg/total      0.833      nan      4208

```

Fig. IV.30. Decision Tree Statistics for All Data

```

===== Confusion Matrix =====
          6_to_10      11_to_15      16_to_20      21_to_25      26_to_30      31_to_35      36_to_40      41_to_45
<- classified as
6_to_10      1141      22      0      0      0      5      0      4
11_to_15      111      912      0      0      0      0      0      13
16_to_20      0      0      0      0      0      0      0      0
21_to_25      0      0      0      0      0      0      0      0
26_to_30      3      0      0      0      11      8      0      0
31_to_35      7      2      0      0      0      526      0      17
36_to_40      0      0      0      0      0      31      0      12
41_to_45      0      0      0      0      0      26      0      303

Total Number of Instances      : 3154
Correctly Classified Instances : 2893
Incorrectly Classified Instances : 261
Kappa Statistic: 0.290802
Accuracy: 91.7248%

Report :      precision      recall      support
6_to_10      0.974      0.904      1172
11_to_15      0.88      0.974      1036
16_to_20      nan      nan      0
21_to_25      nan      nan      0
26_to_30      0.5      1      22
31_to_35      0.953      0.883      552
36_to_40      0      nan      43
41_to_45      0.921      0.868      329

avg/total      0.917      nan      3154

```

Fig. IV.31. Confusion Matrix and Accuracy for Participant 1, 2, and 3 Data

| ===== Confusion Matrix ===== | | | | | | | | |
|----------------------------------|----------|----------|----------|----------|----------|----------|----------|----------|
| | 6_to_10 | 11_to_15 | 16_to_20 | 21_to_25 | 26_to_30 | 31_to_35 | 36_to_40 | 41_to_45 |
| <- classified as | 6_to_10 | 11_to_15 | 16_to_20 | 21_to_25 | 26_to_30 | 31_to_35 | 36_to_40 | 41_to_45 |
| 6_to_10 | 0 | 196 | 0 | 0 | 0 | 0 | 0 | 0 |
| 11_to_15 | 0 | 1693 | 0 | 0 | 0 | 3 | 0 | 1 |
| 16_to_20 | 0 | 66 | 0 | 0 | 0 | 0 | 0 | 0 |
| 21_to_25 | 0 | 0 | 0 | 0 | 0 | 0 | 0 | 0 |
| 26_to_30 | 0 | 13 | 0 | 0 | 0 | 9 | 0 | 0 |
| 31_to_35 | 0 | 10 | 0 | 0 | 0 | 579 | 0 | 7 |
| 36_to_40 | 0 | 0 | 0 | 0 | 0 | 41 | 2 | 0 |
| 41_to_45 | 0 | 0 | 0 | 0 | 108 | 0 | 221 | |
| Total Number of Instances | : 2949 | | | | | | | |
| Correctly Classified Instances | : 2495 | | | | | | | |
| Incorrectly Classified Instances | : 454 | | | | | | | |
| Kappa Statistic: | 0.445362 | | | | | | | |
| Accuracy: | 84.6049% | | | | | | | |

Fig. IV.32. Confusion Matrix and Accuracy for Participant 1, 2, and 4 Data

| ===== Confusion Matrix ===== | | | | | | | | |
|----------------------------------|----------|----------|----------|----------|----------|----------|----------|----------|
| | 6_to_10 | 11_to_15 | 16_to_20 | 21_to_25 | 26_to_30 | 31_to_35 | 36_to_40 | 41_to_45 |
| <- classified as | 6_to_10 | 11_to_15 | 16_to_20 | 21_to_25 | 26_to_30 | 31_to_35 | 36_to_40 | 41_to_45 |
| 6_to_10 | 1255 | 0 | 0 | 0 | 89 | 0 | 0 | |
| 11_to_15 | 481 | 322 | 0 | 0 | 34 | 0 | 0 | |
| 16_to_20 | 44 | 0 | 22 | 0 | 0 | 0 | 0 | |
| 21_to_25 | 0 | 0 | 0 | 0 | 0 | 0 | 0 | |
| 26_to_30 | 2 | 0 | 0 | 0 | 20 | 0 | 0 | |
| 31_to_35 | 4 | 0 | 0 | 0 | 0 | 592 | 0 | 0 |
| 36_to_40 | 0 | 0 | 0 | 0 | 0 | 43 | 0 | 0 |
| 41_to_45 | 0 | 0 | 0 | 0 | 329 | 0 | 0 | |
| Total Number of Instances | : 3237 | | | | | | | |
| Correctly Classified Instances | : 2191 | | | | | | | |
| Incorrectly Classified Instances | : 1046 | | | | | | | |
| Kappa Statistic: | 0.317911 | | | | | | | |
| Accuracy: | 67.6861% | | | | | | | |

Fig. IV.33. Confusion Matrix and Accuracy for Participant 2, 3, and 4 Data

| ===== Confusion Matrix ===== | | | | | | | | |
|----------------------------------|----------|---------|----------|----------|----------|----------|----------|----------|
| | 11_to_15 | 6_to_10 | 16_to_20 | 21_to_25 | 26_to_30 | 31_to_35 | 36_to_40 | 41_to_45 |
| <- classified as | 11_to_15 | 6_to_10 | 16_to_20 | 21_to_25 | 26_to_30 | 31_to_35 | 36_to_40 | 41_to_45 |
| 11_to_15 | 901 | 525 | 0 | 0 | 0 | 0 | 0 | 0 |
| 6_to_10 | 24 | 1343 | 0 | 0 | 0 | 0 | 0 | 0 |
| 16_to_20 | 0 | 44 | 22 | 0 | 0 | 0 | 0 | 0 |
| 21_to_25 | 0 | 0 | 0 | 0 | 0 | 0 | 0 | 0 |
| 26_to_30 | 0 | 0 | 0 | 0 | 0 | 0 | 0 | 0 |
| 31_to_35 | 0 | 0 | 0 | 0 | 0 | 0 | 0 | 0 |
| 36_to_40 | 0 | 0 | 0 | 0 | 0 | 0 | 0 | 0 |
| 41_to_45 | 0 | 0 | 0 | 0 | 0 | 0 | 0 | 0 |
| Total Number of Instances | : 2859 | | | | | | | |
| Correctly Classified Instances | : 2266 | | | | | | | |
| Incorrectly Classified Instances | : 593 | | | | | | | |
| Kappa Statistic: | 0.481314 | | | | | | | |
| Accuracy: | 79.2585% | | | | | | | |

Fig. IV.34. Confusion Matrix and Accuracy for Participant 1, 3, and 4 Data

V. FINDINGS AND RECOMMENDATIONS

Respiration results of all subjects are presented here. The respiratory patterns differ from the patterns captured by the commercial respiration system NeuLog Neuron Logger Sensors NUL-236 Respiration Monitor Belt Logger Sensor. The data collected contained higher levels of noise, likely due to internal limitations with the SensorTile.box PRO as well as the electrode-wire system. To smooth the signals, different filters were tested. Furthermore, it is recommended that future work incorporate additional hardware to achieve ECG functionality utilizing the SensorTile.box PRO. This would allow the end user to more accurately collect heart and respiratory signals.

A. Impact of Posture and Activity

The participant data was collected in 3 positions: sitting, standing and walking. It was found that the subjects had a range of respiratory rates. In particular, subject 2 tended to breathe at a faster rate than average (V.2), and subject 3 tended to breathe at a slightly slower rate than average (V.3).

Between sitting and standing positions, standing postures tended to yield slightly elevated breathing rates, but not elevated enough to detect the difference using the proposed system. This can likely be attributed to increased lung volumes of subjects in standing position due to an increase in volume of the chest cavity. This is most noted in subject 2.

Sitting positions also seemed to yield the lowest levels of noise. This is likely due to the fact that sitting allowed all

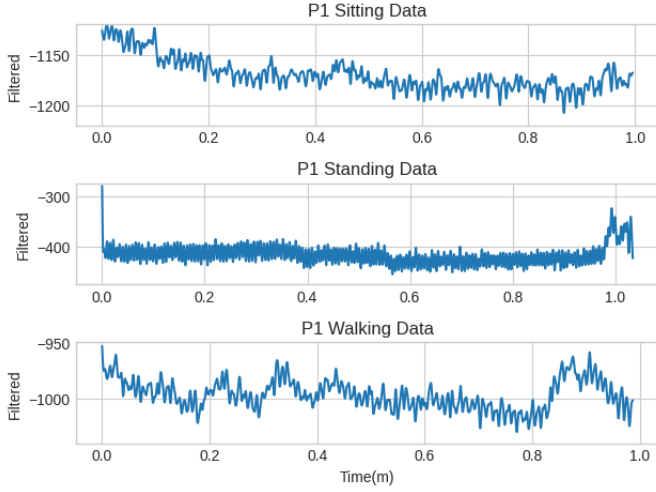


Fig. V.1. Person 1 Sitting, Standing, and Walking Data Sample Comparison

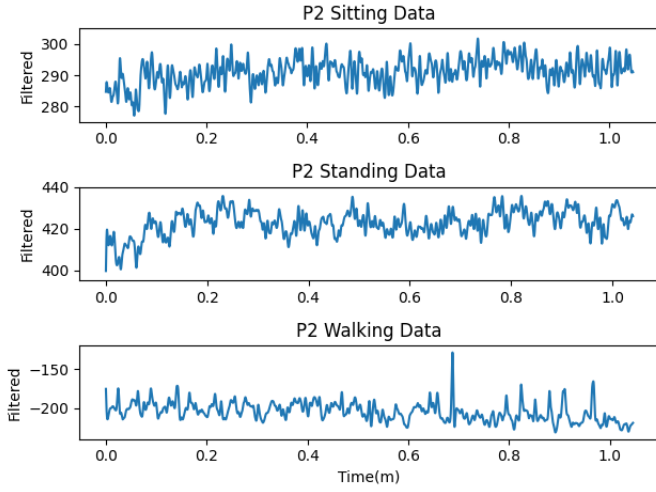


Fig. V.2. Person 2 Sitting, Standing, and Walking Data Sample Comparison

participants to restrict their movements the most, so the least amount of noise was introduced from movement.

Walking activity presented the noisiest patterns compared to standing and sitting. Due to the physical activity, noticeable changes in physiological systems were expected, including breathing. It was noted that although the noise levels were increased, accurate breathing patterns were able to be detected and categorized into specific ranges with 83.29% accuracy.

Because of the relatively slow walking activity collected, it is recommended that further research be conducted to determine the change in breathing patterns with higher intensity physical activity. It is also suggested to compare data from subjects who are talking, as speech often affects breathing cycles.

B. Impact of Gender

It was noted that across the small sample size (4 users), the subjects saw almost no difference. Typically, lung volume

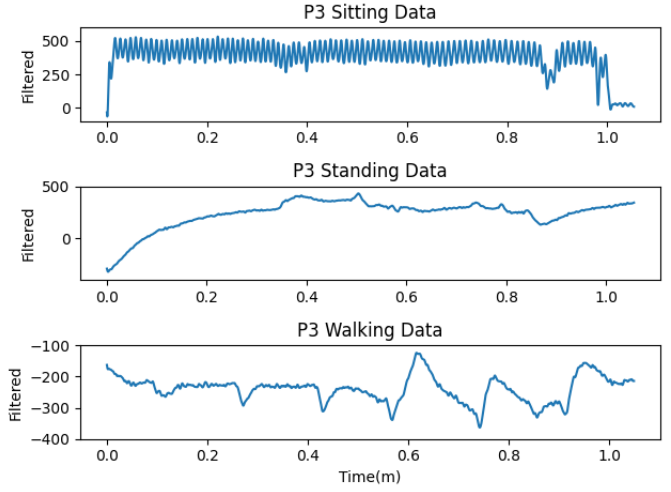


Fig. V.3. Person 3 Sitting, Standing, and Walking Data Sample Comparison

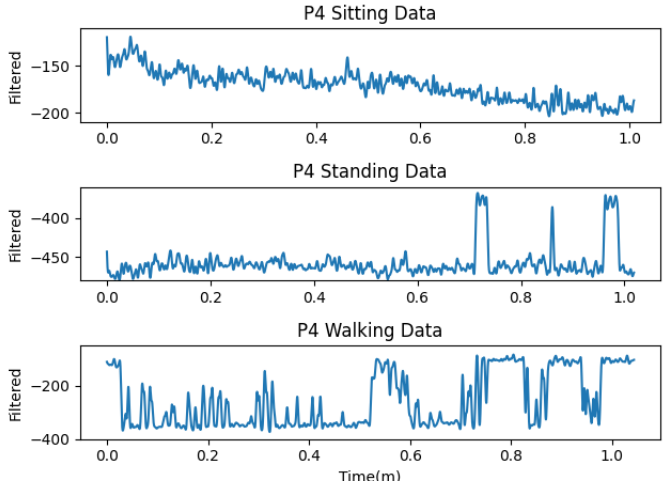


Fig. V.4. Person 4 Sitting, Standing, and Walking Data Sample Comparison

of an adult female is 10%-12% lower than that of a male with the same height and age [2]. While the obtained data did not show any significant differences in breathing rates across gender, studies like the one conducted by Romei et al. have also concluded that the link between gender and lung volume is controversial and may vary [10].

C. Individuality of Breathing Patterns

As dozens of samples per subject were recorded, it was discovered that the physiology of the subjects directly impacted the breathing patterns. With such a small sample size, it is difficult to determine exactly how these cycles differed between subjects, as shown in V.1, V.2, V.3, and V.4 above. In future studies, it is recommended to leverage a larger sample size to determine whether height, weight or other factors tend to produce greater or fewer breaths per minute.

D. Other Potential Factors & Limitations

It is also important to note that other factors may have had an impact on the data collected in this experiment. Almost all of the data collected was taken between the hours of 6 PM and midnight. A smaller amount of data was collected between the hours of 10 AM and 4 PM, but time of day appears to have little to no impact on the data (V.5). However, further analysis could be warranted to determine if respiratory rate changes in individuals throughout the day.

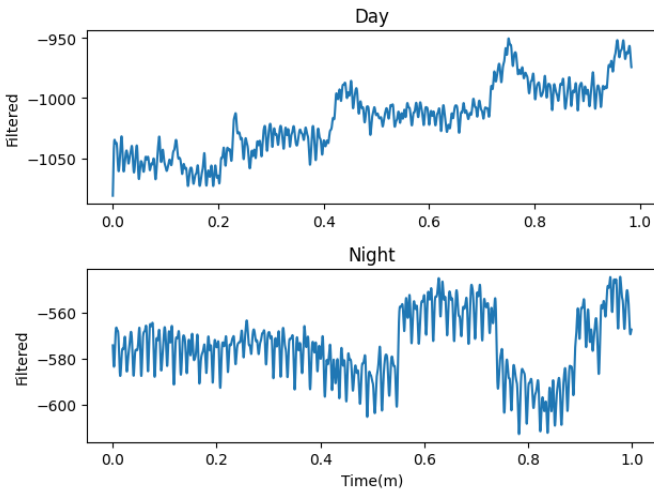


Fig. V.5. Person 1 Sitting Samples at Two Different Times of Day

The experiment was repeated over the course of a two-month period and found that there was little variation in subjects across days. However, it was noted that there was some difficulty producing repeatable results (V.6). This should be taken into account with future studies as well.

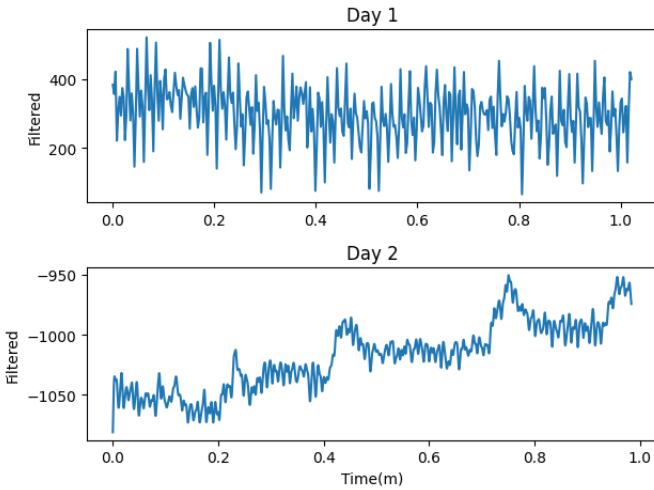


Fig. V.6. Person 1 Sitting Samples on Two Different Days

As the study was conducted, it was found that beyond noise stemming from motion or the device, there were also changes due to the subject's clothing. Participants changed apparel

between sample collection days, which likely affected noise levels between the wire and electrode system. It was found that thinner clothing could occasionally act as a conductive surface and produce further noise (V.7). Thicker fabrics and tighter clothing often produced better results.

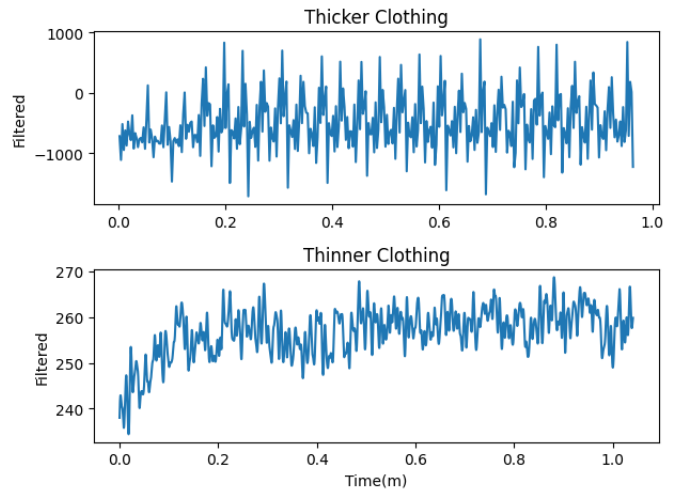


Fig. V.7. Person 2 sitting samples wearing different types of clothing

E. Overall Findings

The study demonstrates a successful, simple way to measure respiration rate with a low-power system. The device has been largely successful in estimating breathing rate, but future work should focus on capturing the breathing patterns as well. There were minimal distinctions in breathing patterns from different positions / activities, and further research with higher intensity activity to help distinguish between them is recommended. Breathing patterns seem relatively unique to individual subjects, so it is recommended that future research work be done to determine exactly which factors (height, weight, gender, etc) are most influential. Although this study was repeated over several sessions with the same and different subjects, some differences between recordings were seen. This is likely due to hardware limitations of the SensorTile.box PRO, so further testing is recommended with additional hardware that includes ECG capabilities. However, these fluctuations did not have any detectable effect on the results.

VI. ACKNOWLEDGMENTS

We would like to express our sincere thanks and gratitude to our Professor, Dr. Mani Srivastava and Gaofeng Dong of the ECE department at the University of California - Los Angeles as well as Dr. Swapnil Sayan Saha and Dr. Mahesh Chowdhary of STMicroelectronics for all their guidance and encouragement throughout the project. Their constant advice and support helped us greatly in our research journey.

REFERENCES

- [1] Angelucci, Alessandra, and Andrea Aliverti. "Telemonitoring Systems for Respiratory Patients: Technological Aspects." *Pulmonology*, no. 4, Elsevier BV, July 2020, pp. 221–32. Crossref, doi:10.1016/j.pulmoe.2019.11.006.

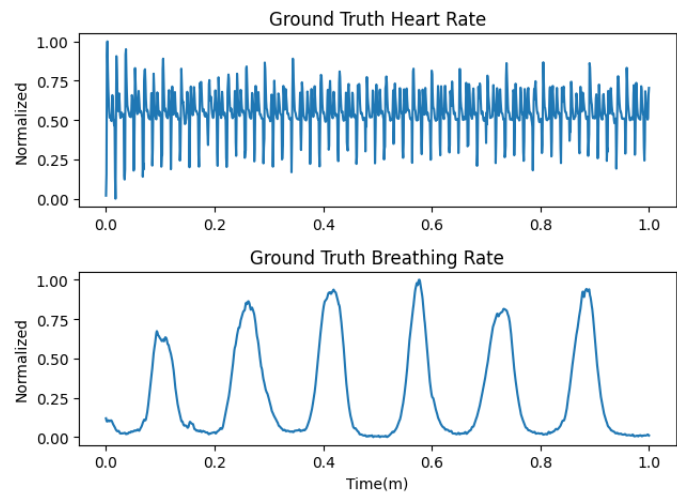
- [2] Bellemare, François, et al. "Sex Differences in Thoracic Dimensions and Configuration." *American Journal of Respiratory and Critical Care Medicine*, no. 3, American Thoracic Society, Aug. 2003, pp. 305–12. Crossref, doi:10.1164/rccm.200208-876oc.
- [3] Chu, Michael, et al. "Respiration Rate and Volume Measurements Using Wearable Strain Sensors." *Npj Digital Medicine*, no. 1, Springer Science and Business Media LLC, Feb. 2019. Crossref, doi:10.1038/s41746-019-0083-3.
- [4] Dhemani, K., et al. "Cardiac monitoring with novel low power sensors measuring upper thoracic electrostatic charge variation for long lasting wearable devices," 2022 18th International Conference on Wireless and Mobile Computing, Networking and Communications (WiMob), 2022, pp. 154-159. Crossref, doi: 10.1109/WiMob55322.2022.9941545.
- [5] Eberlein, Michael, et al. "Chest Wall Strapping. An Old Physiology Experiment with New Relevance to Small Airways Diseases - PMC." PubMed Central (PMC), National Library of Medicine, Oct. 2014, <https://www.ncbi.nlm.nih.gov/pmc/articles/PMC5469355/>.
- [6] Fakir, Y., et al. "Study of The ID3 and C4.5 Learning Algorithms." *Journal of Medical Informatics and Decision Making*, edited by Erfan Babaee, no. 2, Open Access Pub, Apr. 2020, pp. 29–43. Crossref, doi:10.14302/issn.2641-5526.jmid-20-3302.
- [7] Manoni, Alessandro, et al. "Long-Term Polygraphic Monitoring through MEMS and Charge Transfer for Low-Power Wearable Applications." *Sensors*, no. 7, MDPI AG, Mar. 2022, p. 2566. Crossref, doi:10.3390/s22072566.
- [8] Massaroni, Carlo, et al. "Contact-Based Methods for Measuring Respiratory Rate." *Sensors*, no. 4, MDPI AG, Feb. 2019, p. 908. Crossref, doi:10.3390/s19040908.
- [9] Raji, Rafiu King, et al. "Knitted Piezoresistive Smart Chest Band and Its Application for Respiration Patterns Assessment." *Journal of Engineered Fibers and Fabrics*, SAGE Publications, Jan. 2019, p. 155892501986847. Crossref, doi:10.1177/1558925019868474.
- [10] Romei, M., et al. "Effects of Gender and Posture on Thoraco-Abdominal Kinematics during Quiet Breathing in Healthy Adults." *Respiratory Physiology & Neurobiology*, no. 3, Elsevier BV, July 2010, pp. 184–91. Crossref, doi:10.1016/j.resp.2010.05.018.
- [11] "SensorTile.Box PRO with Multi-Sensors and Wireless Connectivity for Any Intelligent IoT Node." STMicroelectronics, STMicroelectronics, www.st.com/en/evaluation-tools/steval-mkboxpro.html.

VII. APPENDIX

A. Github Repository

https://github.com/Naya-K-M/QVAR_Capstone_2

B. Ground Truth Data Sample



C. Machine Learning Additional Models (Attached Below)

```

F8_PeakToPeak_on_filter_DIFF_on_A_X <= 0.0895144: 11_to_15 (891.0/24.0)
F8_PeakToPeak_on_filter_DIFF_on_A_X > 0.0895144
|   F5_ENERGY_on_ACC_X <= 13.3742
|   |   F21_MIN_on_ACC_X <= -0.23999
|   |   |   F11_PositiveZeroCross_on_ACC_X <= 122
|   |   |   |   F5_ENERGY_on_ACC_X <= 4.02734
|   |   |   |   |   F1_MEAN_on_ACC_X <= -0.0947876: 31_to_35 (16.0)
|   |   |   |   |   F1_MEAN_on_ACC_X > -0.0947876: 11_to_15 (4.0)
|   |   |   |   F5_ENERGY_on_ACC_X > 4.02734
|   |   |   |   |   F16_PeaKDet_on_filter_DIFF_on_A_X <= 185: 6_to_10 (51.0)
|   |   |   |   |   F16_PeaKDet_on_filter_DIFF_on_A_X > 185
|   |   |   |   |   |   F1_MEAN_on_ACC_X <= -0.00587082
|   |   |   |   |   |   |   F2_MEAN_on_filter_DIFF_on_A_X <= -0.000993729: 6_to_10 (1.0)
|   |   |   |   |   |   |   F2_MEAN_on_filter_DIFF_on_A_X > -0.000993729: 31_to_35 (4.0)
|   |   |   |   |   |   F1_MEAN_on_ACC_X > -0.00587082
|   |   |   |   |   |   |   F2_MEAN_on_filter_DIFF_on_A_X <= -0.000413656: 11_to_15 (4.0)
|   |   |   |   |   |   |   F2_MEAN_on_filter_DIFF_on_A_X > -0.000413656
|   |   |   |   |   |   |   |   F1_MEAN_on_ACC_X <= 0.047821: 6_to_10 (5.0)
|   |   |   |   |   |   |   |   F1_MEAN_on_ACC_X > 0.047821
|   |   |   |   |   |   |   |   |   F1_MEAN_on_ACC_X <= 0.0734863: 11_to_15 (2.0)
|   |   |   |   |   |   |   |   |   F1_MEAN_on_ACC_X > 0.0734863: 6_to_10 (1.0)
|   |   |   |   |   F11_PositiveZeroCross_on_ACC_X > 122
|   |   |   |   |   |   F1_MEAN_on_ACC_X <= 0.029125: 31_to_35 (261.0/13.0)
|   |   |   |   |   |   F1_MEAN_on_ACC_X > 0.029125
|   |   |   |   |   |   |   F15_PeaKDet_on_ACC_X <= 164
|   |   |   |   |   |   |   |   F4_VAR_on_filter_DIFF_on_A_X <= 0.0234222: 6_to_10 (3.0)
|   |   |   |   |   |   |   |   F4_VAR_on_filter_DIFF_on_A_X > 0.0234222: 25_to_30 (11.0)
|   |   |   |   |   |   |   F15_PeaKDet_on_ACC_X > 164
|   |   |   |   |   |   |   |   F1_MEAN_on_ACC_X <= 0.0351563: 31_to_35 (5.0)
|   |   |   |   |   |   |   |   F1_MEAN_on_ACC_X > 0.0351563: 11_to_15 (3.0)
|   |   |   |   F21_MIN_on_ACC_X > -0.23999
|   |   |   |   |   F5_ENERGY_on_ACC_X <= 1.27926
|   |   |   |   |   |   F7_PeakToPeak_on_ACC_X <= 0.223877: 31_to_35 (237.0/57.0)
|   |   |   |   |   |   F7_PeakToPeak_on_ACC_X > 0.223877
|   |   |   |   |   |   |   F1_MEAN_on_ACC_X <= -0.0401611
|   |   |   |   |   |   |   |   F1_MEAN_on_ACC_X <= -0.0471497: 41_to_45 (14.0)
|   |   |   |   |   |   |   |   F1_MEAN_on_ACC_X > -0.0471497
|   |   |   |   |   |   |   |   |   F2_MEAN_on_filter_DIFF_on_A_X <= 0: 41_to_45 (2.0)
|   |   |   |   |   |   |   |   |   F2_MEAN_on_filter_DIFF_on_A_X > 0: 31_to_35 (3.0)
|   |   |   |   |   |   |   |   F1_MEAN_on_ACC_X > -0.0401611
|   |   |   |   |   |   |   |   |   F1_MEAN_on_ACC_X <= -0.0114517: 6_to_10 (1.0)
|   |   |   |   |   |   |   |   |   F1_MEAN_on_ACC_X > -0.0114517: 11_to_15 (8.0)
|   |   |   |   |   |   F5_ENERGY_on_ACC_X > 1.27926: 41_to_45 (287.0/46.0)
|   |   |   |   F5_ENERGY_on_ACC_X > 13.3742: 6_to_10 (1079.0/121.0)

```

Number of Leaves : 23
Size of the tree : 45

Fig. VII.1. Decision Tree for Participant 1, 2, and 3

```

class:
=> 6_to_10, 11_to_15, 16_to_20, 21_to_25, 25_to_30, 31_to_35, 36_to_40, 41_to_45,
features:
=> F1_MEAN_on_ACC_X, F2_MEAN_on_filter_DIFF_on_A_X, F3_VAR_on_ACC_X, F4_VAR_on_filter_DIFF_on_A_X, F5_ENERGY_on_ACC_X, F6
 ENERGY_on_filter_DIFF_on_A_X, F7_PeakToPeak_on_ACC_X, F8_PeakToPeak_on_filter_DIFF_on_A_X, F9_ZeroCross_on_ACC_X, F10
 ZeroCross_on_filter_DIFF_on_A_X, F11_PositiveZeroCross_on_ACC_X, F12_PositiveZeroCross_on_filter_DIFF_on_A_X, F13
 NegativeZeroCross_on_ACC_X, F14_NegativeZeroCross_on_filter_DIFF_on_A_X, F15_PeakDet_on_ACC_X, F16_PeakDet_on_filter_DIFF_on_A_X, F17
 PosPeakDet_on_ACC_X, F18_PosPeakDet_on_filter_DIFF_on_A_X, F19_NegPeakDet_on_ACC_X, F20_NegPeakDet_on_filter_DIFF_on_A_X, F21
 MIN_on_ACC_X, F22_MIN_on_filter_DIFF_on_A_X, F23_MAX_on_ACC_X, F24_MAX_on_filter_DIFF_on_A_X, F25_RECURSIVE_FEATURE_MEAN_on_ACC_X, F26
 RECURSIVE_FEATURE_VAR_on_ACC_X, F27_RECURSIVE_FEATURE_RMS_on_ACC_X, F28_RECURSIVE_FEATURE_MEAN_on_filter_DIFF_on_A_X, F29
 RECURSIVE_FEATURE_VAR_on_filter_DIFF_on_A_X, F30_RECURSIVE_FEATURE_RMS_on_filter_DIFF_on_A_X, F31_RECURSIVE_FEATURE_MAX_on_ACC_X, F32
 RECURSIVE_FEATURE_MIN_on_ACC_X, F33_RECURSIVE_FEATURE_PKPK_on_ACC_X, F34_RECURSIVE_FEATURE_MAX_on_filter_DIFF_on_A_X, F35
 RECURSIVE_FEATURE_MIN_on_filter_DIFF_on_A_X, F36_RECURSIVE_FEATURE_PKPK_on_filter_DIFF_on_A_X,
Mean absolute error      0.915748
Root mean squared error 0.915876
===== Whole data training with Confidence Factor: 0.9 =====

===== Confusion Matrix =====
          6_to_10      11_to_15      16_to_20      21_to_25      25_to_30      31_to_35      36_to_40      41_to_45
    <- classified as
6_to_10        1141       22       0       0       0       5       0       4
11_to_15        111       912       0       0       0       0       0      13
16_to_20         0       0       0       0       0       0       0       0
21_to_25         0       0       0       0       0       0       0       0
25_to_30         3       0       0       0      11       8       0       0
31_to_35         7       2       0       0       0      526       0      17
36_to_40         0       0       0       0       0      31       0      12
41_to_45         0       0       0       0       0      26       0     303

Total Number of Instances      : 3154
Correctly Classified Instances : 2893
Incorrectly Classified Instances : 261
Kappa Statistic: 0.290802
Accuracy: 91.7248%

Report :
      precision    recall   support
6_to_10      0.974    0.904    1172
11_to_15     0.88     0.974    1036
16_to_20     nan      nan      0
21_to_25     nan      nan      0
25_to_30     0.5      1       22
31_to_35     0.953    0.883    552
36_to_40     0       nan      43
41_to_45     0.921    0.868    329
avg/total    0.917    nan     3154

```

Fig. VII.2. Decision Tree Statistics for Participant 1, 2, and 3

```

F1_MEAN_on_ACC_X <= 0.0262392
| F9_ZeroCross_on_ACC_X <= 204.054
| | F1_MEAN_on_ACC_X <= -0.0570958: 41_to_45 (203.0/8.0)
| | F1_MEAN_on_ACC_X > -0.0570958
| | | F3_VAR_on_ACC_X <= 0.00134468
| | | | F22_MIN_on_filter_DIFF_on_A_X <= -0.0559692: 31_to_35 (21.0)
| | | | F22_MIN_on_filter_DIFF_on_A_X > -0.0559692
| | | | | F32_RECURSIVE_FEATURE_MIN_on_ACC_X <= -0.0791626: 31_to_35 (5.0)
| | | | | F32_RECURSIVE_FEATURE_MIN_on_ACC_X > -0.0791626
| | | | | | F1_MEAN_on_ACC_X <= -0.0532532: 36_to_40 (2.0)
| | | | | | F1_MEAN_on_ACC_X > -0.0532532: 11_to_15 (1.0)
| | | | F3_VAR_on_ACC_X > 0.00134468
| | | | | F1_MEAN_on_ACC_X <= -0.0446167: 41_to_45 (18.0)
| | | | | F1_MEAN_on_ACC_X > -0.0446167
| | | | | | F1_MEAN_on_ACC_X <= -0.022049: 31_to_35 (2.0)
| | | | | | F1_MEAN_on_ACC_X > -0.022049: 11_to_15 (9.0)
| | F9_ZeroCross_on_ACC_X > 204.054: 31_to_35 (551.0/161.0)
F1_MEAN_on_ACC_X > 0.0262392: 11_to_15 (1683.0/285.0)

Number of Leaves :      10
Size of the tree :     19

```

Fig. VII.3. Decision Tree for Participant 1, 2, and 4

```

class:
=> 6_to_10, 11_to_15, 16_to_20, 21_to_25, 26_to_30, 31_to_35, 36_to_40, 41_to_45,
features:
=> F1_MEAN_on_ACC_X, F2_MEAN_on_filter_DIFF_on_A_X, F3_VAR_on_ACC_X, F4_VAR_on_filter_DIFF_on_A_X, F5_ENERGY_on_ACC_X, F6
 ENERGY_on_filter_DIFF_on_A_X, F7_PeakToPeak_on_ACC_X, F8_PeakToPeak_on_filter_DIFF_on_A_X, F9_ZeroCross_on_ACC_X, F10
 _ZeroCross_on_filter_DIFF_on_A_X, F11_PositiveZeroCross_on_ACC_X, F12_PositiveZeroCross_on_filter_DIFF_on_A_X, F13
 _NegativeZeroCross_on_ACC_X, F14_NegativeZeroCross_on_filter_DIFF_on_A_X, F15_PeakDet_on_ACC_X, F16_PeakDet_on_filter_DIFF_on_A_X, F17
 PosPeakDet_on_ACC_X, F18_PosPeakDet_on_filter_DIFF_on_A_X, F19_NegPeakDet_on_ACC_X, F20_NegPeakDet_on_filter_DIFF_on_A_X, F21
 _MIN_on_ACC_X, F22_MIN_on_filter_DIFF_on_A_X, F23_MAX_on_ACC_X, F24_MAX_on_filter_DIFF_on_A_X, F25_RECURSIVE_FEATURE_MEAN_on_ACC_X, F26
 _RECURSIVE_FEATURE_VAR_on_ACC_X, F27_RECURSIVE_FEATURE_RMS_on_ACC_X, F28_RECURSIVE_FEATURE_MEAN_on_filter_DIFF_on_A_X, F29
 _RECURSIVE_FEATURE_VAR_on_filter_DIFF_on_A_X, F30_RECURSIVE_FEATURE_RMS_on_filter_DIFF_on_A_X, F31_RECURSIVE_FEATURE_MAX_on_ACC_X, F32
 _RECURSIVE_FEATURE_MIN_on_ACC_X, F33_RECURSIVE_FEATURE_PKPK_on_ACC_X, F34_RECURSIVE_FEATURE_MAX_on_filter_DIFF_on_A_X, F35
 _RECURSIVE_FEATURE_MIN_on_filter_DIFF_on_A_X, F36_RECURSIVE_FEATURE_PKPK_on_filter_DIFF_on_A_X,

Mean absolute error      0.864849
Root mean squared error 0.864993
===== Whole data training with Confidence Factor: 0.9 =====

===== Confusion Matrix =====
          6_to_10      11_to_15      16_to_20      21_to_25      26_to_30      31_to_35      36_to_40      41_to_45
    <-- classified as
6_to_10      0       196       0       0       0       0       0       0
11_to_15     0      1693       0       0       0       3       0       1
16_to_20      0       66       0       0       0       0       0       0
21_to_25     0       0       0       0       0       0       0       0
26_to_30     0       13       0       0       0       9       0       0
31_to_35     0       10       0       0       0       579      0       7
36_to_40     0       0       0       0       0       41       2       0
41_to_45     0       0       0       0       0      108      0      221

Total Number of Instances      : 2949
Correctly Classified Instances : 2495
Incorrectly Classified Instances : 454
Kappa Statistic: 0.445362
Accuracy: 84.6049%


Report :
  precision    recall  support
6_to_10        0     nan     196
11_to_15      0.998   0.856   1697
16_to_20        0     nan      66
21_to_25        nan    nan      0
26_to_30        0     nan     22
31_to_35      0.971   0.782   596
36_to_40      0.0465    1     43
41_to_45      0.672   0.965   329

avg/total      0.846     nan    2949

```

Fig. VII.4. Decision Tree Statistics for Participant 1, 2, and 4

```

F5_ENERGY_on_ACC_X <= 13.8532: 31_to_35 (592.0/515.0)
F5_ENERGY_on_ACC_X > 13.8532
|   F22_MIN_on_filter_DIFF_on_A_X <= -0.05664: 6_to_10 (1247.0/531.0)
|   F22_MIN_on_filter_DIFF_on_A_X > -0.05664
|       F1_MEAN_on_ACC_X <= 0.306457
|           F1_MEAN_on_ACC_X <= 0.295654
|               F1_MEAN_on_ACC_X <= -0.27124: 6_to_10 (8.0)
|               F1_MEAN_on_ACC_X > -0.27124: 11_to_15 (36.0)
|           F1_MEAN_on_ACC_X > 0.295654
|               F30_RECURSIVE_FEATURE_RMS_on_filter_DIFF_on_A_X <= 0.00595022: 16_to_20 (13.0)
|               F30_RECURSIVE_FEATURE_RMS_on_filter_DIFF_on_A_X > 0.00595022
|                   F30_RECURSIVE_FEATURE_RMS_on_filter_DIFF_on_A_X <= 0.0124104: 11_to_15 (5.0)
|                   F30_RECURSIVE_FEATURE_RMS_on_filter_DIFF_on_A_X > 0.0124104
|                       F1_MEAN_on_ACC_X <= 0.303467: 16_to_20 (8.0)
|                       F1_MEAN_on_ACC_X > 0.303467
|                           F1_MEAN_on_ACC_X <= 0.304932: 11_to_15 (2.0)
|                           F1_MEAN_on_ACC_X > 0.304932: 16_to_20 (1.0)
|       F1_MEAN_on_ACC_X > 0.306457: 11_to_15 (279.0)

Number of Leaves :      10
Size of the tree :    19

```

Fig. VII.5. Decision Tree for Participant 2, 3, and 4

```

class:
=> 6_to_10, 11_to_15, 16_to_20, 21_to_25, 26_to_30, 31_to_35, 36_to_40, 41_to_45,
features:
=> F1_MEAN_on_ACC_X, F2_MEAN_on_filter_DIFF_on_A_X, F3_VAR_on_ACC_X, F4_VAR_on_filter_DIFF_on_A_X, F5_ENERGY_on_ACC_X, F6
_ENERGY_on_filter_DIFF_on_A_X, F7_PeakToPeak_on_ACC_X, F8_PeakToPeak_on_filter_DIFF_on_A_X, F9_ZeroCross_on_ACC_X, F10
_ZeroCross_on_filter_DIFF_on_A_X, F11_PositiveZeroCross_on_ACC_X, F12_PositiveZeroCross_on_filter_DIFF_on_A_X, F13
_NegativeZeroCross_on_ACC_X, F14_NegativeZeroCross_on_filter_DIFF_on_A_X, F15_PeakDet_on_ACC_X, F16_PeakDet_on_filter_DIFF_on_A_X, F17
_PosPeakDet_on_ACC_X, F18_PosPeakDet_on_filter_DIFF_on_A_X, F19_NegPeakDet_on_ACC_X, F20_NegPeakDet_on_filter_DIFF_on_A_X, F21
_MIN_on_ACC_X, F22_MIN_on_filter_DIFF_on_A_X, F23_MAX_on_ACC_X, F24_MAX_on_filter_DIFF_on_A_X, F25_RECURSIVE_FEATURE_MEAN_on_ACC_X, F26
_RECURSIVE_FEATURE_VAR_on_ACC_X, F27_RECURSIVE_FEATURE_RMS_on_ACC_X, F28_RECURSIVE_FEATURE_MEAN_on_filter_DIFF_on_A_X, F29
_RECURSIVE_FEATURE_VAR_on_filter_DIFF_on_A_X, F30_RECURSIVE_FEATURE_RMS_on_filter_DIFF_on_A_X, F31_RECURSIVE_FEATURE_MAX_on_ACC_X, F32
_RECURSIVE_FEATURE_MIN_on_ACC_X, F33_RECURSIVE_FEATURE_PKPK_on_ACC_X, F34_RECURSIVE_FEATURE_MAX_on_filter_DIFF_on_A_X, F35
_RECURSIVE_FEATURE_MIN_on_filter_DIFF_on_A_X, F36_RECURSIVE_FEATURE_PKPK_on_filter_DIFF_on_A_X,

Mean absolute error      0.720472
Root mean squared error 0.725695
===== Whole data training with Confidence Factor: 0.9 =====

===== Confusion Matrix =====
          6_to_10      11_to_15      16_to_20      21_to_25      26_to_30      31_to_35      36_to_40      41_to_45
<-- classified as
6_to_10      1255      0      0      0      89      0      0
11_to_15      481      322      0      0      0      34      0      0
16_to_20      44      0      22      0      0      0      0      0
21_to_25      0      0      0      0      0      0      0      0
26_to_30      2      0      0      0      0      20      0      0
31_to_35      4      0      0      0      0      592      0      0
36_to_40      0      0      0      0      0      43      0      0
41_to_45      0      0      0      0      0      329      0      0

Total Number of Instances      : 3237
Correctly Classified Instances : 2191
Incorrectly Classified Instances : 1046
Kappa Statistic: 0.317911
Accuracy: 67.6861%

Report :
          precision    recall  support
6_to_10      0.934     0.703   1344
11_to_15      0.385      1     837
16_to_20      0.333      1     66
21_to_25      nan       nan     0
26_to_30      0         nan     22
31_to_35      0.993     0.535   596
36_to_40      0         nan     43
41_to_45      0         nan    329

avg/total    0.677      nan    3237

```

Fig. VII.6. Decision Tree Statistics for Participant 2, 3, and 4

```

F8_PeakToPeak_on_filter_DIFF_on_A_X <= 0.0983843
|   F5_ENERGY_on_ACC_X <= 22.5441: 11_to_15 (887.0/24.0)
|   F5_ENERGY_on_ACC_X > 22.5441
|       F1_MEAN_on_ACC_X <= 0.306396
|           F1_MEAN_on_ACC_X <= 0.298828
|               F1_MEAN_on_ACC_X <= 0.296387: 16_to_20 (1.0)
|               F1_MEAN_on_ACC_X > 0.296387: 11_to_15 (4.0)
|           F1_MEAN_on_ACC_X > 0.298828
|               F9_ZeroCross_on_ACC_X <= 98: 11_to_15 (1.0)
|               F9_ZeroCross_on_ACC_X > 98: 16_to_20 (21.0)
|       F1_MEAN_on_ACC_X > 0.306396: 11_to_15 (9.0)
F8_PeakToPeak_on_filter_DIFF_on_A_X > 0.0983843
|   F1_MEAN_on_ACC_X <= 0.0123489: 6_to_10 (557.0/2.0)
|   F1_MEAN_on_ACC_X > 0.0123489: 6_to_10 (786.0/567.0)

Number of Leaves :      8
Size of the tree :     15

```

Fig. VII.7. Decision Tree for Participant 1, 3, and 4

```

class:
=> 11_to_15, 6_to_10, 16_to_20, 21_to_25, 26_to_30, 31_to_35, 36_to_40, 41_to_45,
features:
=> F1_MEAN_on_ACC_X, F2_MEAN_on_filter_DIFF_on_A_X, F3_VAR_on_ACC_X, F4_VAR_on_filter_DIFF_on_A_X, F5_ENERGY_on_ACC_X, F6
_ENERGY_on_filter_DIFF_on_A_X, F7_PeakToPeak_on_ACC_X, F8_PeakToPeak_on_filter_DIFF_on_A_X, F9_ZeroCross_on_ACC_X, F10
_ZeroCross_on_filter_DIFF_on_A_X, F11_PositiveZeroCross_on_ACC_X, F12_PositiveZeroCross_on_filter_DIFF_on_A_X, F13
_NegativeZeroCross_on_ACC_X, F14_NegativeZeroCross_on_filter_DIFF_on_A_X, F15_PeaKDet_on_ACC_X, F16_PeaKDet_on_filter_DIFF_on_A_X, F17
_PosPeaKDet_on_ACC_X, F18_PosPeaKDet_on_filter_DIFF_on_A_X, F19_NegPeaKDet_on_ACC_X, F20_NegPeaKDet_on_filter_DIFF_on_A_X, F21
_MIN_on_ACC_X, F22_MIN_on_filter_DIFF_on_A_X, F23_MAX_on_ACC_X, F24_MAX_on_filter_DIFF_on_A_X, F25_RECURSIVE_FEATURE_MEAN_on_ACC_X, F26
_RECURSIVE_FEATURE_VAR_on_ACC_X, F27_RECURSIVE_FEATURE_RMS_on_ACC_X, F28_RECURSIVE_FEATURE_MEAN_on_filter_DIFF_on_A_X, F29
_RECURSIVE_FEATURE_VAR_on_filter_DIFF_on_A_X, F30_RECURSIVE_FEATURE_RMS_on_filter_DIFF_on_A_X, F31_RECURSIVE_FEATURE_MAX_on_ACC_X, F32
_RECURSIVE_FEATURE_MIN_on_ACC_X, F33_RECURSIVE_FEATURE_PKPK_on_ACC_X, F34_RECURSIVE_FEATURE_MAX_on_filter_DIFF_on_A_X, F35
_RECURSIVE_FEATURE_MIN_on_filter_DIFF_on_A_X, F36_RECURSIVE_FEATURE_PKPK_on_filter_DIFF_on_A_X

Mean absolute error      0.818976
Root mean squared error 0.819439
===== Whole data training with Confidence Factor: 0.9 =====

===== Confusion Matrix =====
          11_to_15      6_to_10      16_to_20      21_to_25      26_to_30      31_to_35      36_to_40      41_to_45
<- classified as
11_to_15      901      525       0       0       0       0       0       0
6_to_10        24      1343       0       0       0       0       0       0
16_to_20        0       44       22       0       0       0       0       0
21_to_25        0       0       0       0       0       0       0       0
26_to_30        0       0       0       0       0       0       0       0
31_to_35        0       0       0       0       0       0       0       0
36_to_40        0       0       0       0       0       0       0       0
41_to_45        0       0       0       0       0       0       0       0

Total Number of Instances      : 2859
Correctly Classified Instances : 2266
Incorrectly Classified Instances : 593
Kappa Statistic: 0.481314
Accuracy: 79.2585%

Report :
      precision    recall   support
11_to_15      0.632     0.974    1426
6_to_10        0.982     0.702    1367
16_to_20      0.333      1       66
21_to_25      nan       nan      0
26_to_30      nan       nan      0
31_to_35      nan       nan      0
36_to_40      nan       nan      0
41_to_45      nan       nan      0

avg/total      0.793     nan     2859

```

Fig. VII.8. Decision Tree Statistics for Participant 1, 3, and 4